Journal of Nuclear Materials 404 (2010) 178–202

Contents lists available at ScienceDirect

Journal of Nuclear Materials

journal homepage: www.elsevier.com/locate/jnucmat

Analytic implementation of the GRAAL model: Application to a R7T7-type glass package in a geological disposal environment

Y. Minet [a,*], B. Bonin [b], S. Gin [a], P. Frugier [a]

[a] CEA Marcoule, DTCD/SECM/LCLT, BP 17171, 30207 Bagnols-sur-Cèze Cedex, France
[b] CEA Saclay, DEN/DIR/DS, 91191 Gif-sur-Yvette Cedex, France

ARTICLE INFO

Article history:
Received 23 February 2010
Accepted 7 July 2010

ABSTRACT

The Glass Reactivity with Allowance for the Alteration Layer Model (GRAAL) was proposed in 2008 to describe borosilicate nuclear glass alteration based on coupling an affinity law with the formation and dissolution of a passivating reactive interface. It is examined here in a simplified form in which only the affinity with respect to silicon is taken into account with a concentration at saturation C_{sat}, and the precipitation of neoformed phases is described by an affine relation for silicon above a precipitation threshold C'_{sat}. This simplified "analytical GRAAL" model is capable of predicting the quantities of altered glass and the silicon and boron concentration variations in analytical or semi-analytical form, and thereby identify the main characteristic quantities of the system. The model was tested against a series of laboratory experiments lasting from a few days to a few years; its sensitivity to the parameter values was examined, and the model was validated with respect to SON68 glass alteration in initially pure water. It was then applied to the alteration of a glass package in a repository over periods of up to a million years, by means of exploratory calculations comprising a sensitivity study of the internal model parameters and extrapolation to the temperatures expected in a geological repository in order to identify the parameters and mechanisms having the greatest impact on the residual alteration rate. Alteration is controlled by the precipitation of neoformed phases in every case. The transient conditions are of very limited duration with respect to either silicon or boron (no more than a 100 years, with less than 0.01% alteration of the package). In the precipitation law used in the model, the residual alteration rate and total package lifetime are determined primarily by two parameters: k' (the precipitation kinetics) and σ' (the precipitate surface area per unit volume in the geological barrier). The package lifetime is about 3×10^5 years at 30 °C assuming a reasonable value for σ' (10^6 m^{-1}), and would be increased by a factor 3–6 if precipitation in the barrier were disregarded. This cursory description of precipitation will be validated and refined through specific laboratory tests at 50 °C and lower temperatures, coordinated with the development of the "geochemical GRAAL" model and with integral tests in contact with clay and canister corrosion products.

1. Introduction

The safety demonstration of a geological disposal for long-lived nuclear wastes implies predicting the waste package evolution over hundreds of thousands of years, and more precisely the evolution of the source term, i.e. flow of radionuclides released from the confinement material over time. In France the long-lived wastes resulting from the spent nuclear fuel reprocessing are confined within a borosilicate glass matrix [1]. Their disposal is set to lay inside the Callovo-Oxfordian argillites of the northeastern Paris Basin [2,3]. The mitigation of the radiological risk associated with the radioactive decay of those wastes occurs on time scales of thousands of years. Direct experimental validation is impossible at such time scales. Establishing the source term therefore requires the use of a model coupling nuclear glass chemistry and the transport of species in the environment, applied to vitrified waste packages in their repository site. Modeling involves establishing relations describing glass alteration as a function of system parameters (especially the temperature, chemical composition, and solution pH at the reaction interface, the glass chemical composition, etc.). These relations are postulated, then validated by laboratory observations (observing the alteration of a glass sample over time under specified conditions) or on natural analogs (studies of alteration on a geological or historical time scale [4–6]). They make it possible to discern the mechanisms controlling glass alteration—at least under controlled conditions (for example glass leaching under static conditions in initially pure water). Some of these controlling mechanisms are responsible for the residual rate regime observed in the laboratory during tests under static

* Corresponding author. Tel.: +33 466791673; fax: +33 466796620.
E-mail address: yves.minet@cea.fr (Y. Minet).

0022-3115/$ - see front matter © 2010 Elsevier B.V. All rights reserved.
doi:10.1016/j.jnucmat.2010.07.015

conditions or with very low flow rates. It is not easy to obtain precise measurements of the characteristics of this regime (alteration rates and their variations according to the glass composition and operating conditions), and yet it is the design basis regime for the long-term package evolution in a geological repository [7].

In the case of R7T7-type glass designed for containment of nuclear waste from French light water reactors, our growing understanding of these controlling mechanisms and especially of those governing the residual rate regime has recently led to the development of a model known as Glass Reactivity with Allowance for the Alteration Layer (GRAAL). This model is described in [8,9] and in Fig. 1; applicable to nuclear borosilicate glasses and initially applied to SON68 glass (inactive R7T7 reference glass, which chemical composition is given in Table 1), it assumes glass alteration is controlled by an amorphous layer consisting of glass no longer containing any mobile elements (alkalis, boron, etc.) and known as the "passivating reactive interphase" (PRI). The term highlights the diffusion barrier role of this layer with respect to the transport of water to the glass and of solvated ions from the glass into solution. The dissolution of the PRI outer face is controlled by an affinity term with respect to its constituents: silicon, aluminum, calcium, zirconium, etc. However, the existence of a passivating barrier protecting the glass by retarding the contact of water, had already been observed on simplified borosilicate glasses [10,11]. The observed effect has been explained by dissolution/recondensation phenomena involving glass network formers, notably silicon, using Monte-Carlo models at an atomistic scale.

As it is based on a main controlling mechanism, the GRAAL model uses simplified hypotheses about the alteration products by describing only the passivating zone of the glass alteration layer (the PRI). The properties of the PRI are described by a single diffusion coefficient governing both water diffusion and the transport of mobile species. In other words, water diffusion through the PRI and diffusion of mobile elements towards the outer solution, are assumed to have similar magnitude and opposite directions. The other elements are assumed to dissolve and, under suitable conditions, precipitate in secondary phases, distinct from the glass alteration layer (the latter being named "gel").

Through these simplifications, the model seeks mainly to describe glass alteration for time durations in which the transient mechanisms due to the complexity of the glass/solution interface have little impact. This is the case for the durations relevant to geological disposal; nevertheless, some limited disagreements with laboratory-scale experimental data are expected, and are to be analysed.

This paper describes an implementation of the GRAAL model based on an additional simplifying hypothesis with respect to chemistry, under which the PRI reactivity, as well as the precipitation of neoformed phases, are assumed to depend only on silicon. This hypothesis, leading to numerous models [12,13], is based on the fact that silicon is the main glass network former. With such basis, however, this model will not assess realistically the consequences of pH variations on the glass alteration [14].

Based on analytical or semi-analytical solutions for the equation system, this approach should make it possible to discern the principal characteristic quantities of the system, not only to describe laboratory tests under static or dynamic conditions, but also for application to alteration of the glass package in a geological repository (assuming that the chemical, thermal and hydrodynamical conditions imposed to the glass could be determined in addition with enough precision). This work proposes, via a sensitivity study, to evaluate the impact of the main model parameters at both space-time scales.

The "analytical GRAAL" model is described in **Part** 2 together with the values assigned to its fundamental parameters. The model predictions are compared in **Part** 3 with the results of laboratory tests of SON68 glass leaching under static and dynamic conditions, notably including the tests used to validate the "geochemical GRAAL" model described in [9]. This approach not only validates the analytical model, but also demonstrates the sensitivity of the predictions to the parameter values at laboratory—i.e. centimeter—scale over time periods ranging from a few days to a few years.

Part 4 discusses the application of the "analytical GRAAL" model to the alteration of a glass package in a geological repository. The calculations were initially performed at 90 °C, i.e. a temperature at which the model can be validated with respect to laboratory tests, first of all in a reference configuration then considering the sensitivity of the parameters in terms of their impact on the long-term behavior of the package and especially its residual alteration rate. The model was then applied to temperatures more representative of glass alteration in a repository, i.e. 30 and 50 °C, based on hypotheses concerning the temperature-dependence of the mechanisms having long-term impact—especially the secondary phase precipitation kinetics.

It is important to note that these calculations applied to a geological repository are not actual package performance assessment calculations, which are now carried out using operational models [15,16]. The main purpose of these calculations is to determine the long-term validity range of the GRAAL model and identify areas in which further research is necessary to reduce the uncertainties on the impact of some controlling phenomena. For example, secondary phase precipitation appears to have a major role in this regard, and yet the parameters describing these phenomena are either difficult to measure on the basis of laboratory leach test results—especially at repository temperatures (20–50 °C)—or are likely to be poorly described by an analytical approach compared with a more detailed chemical approach.

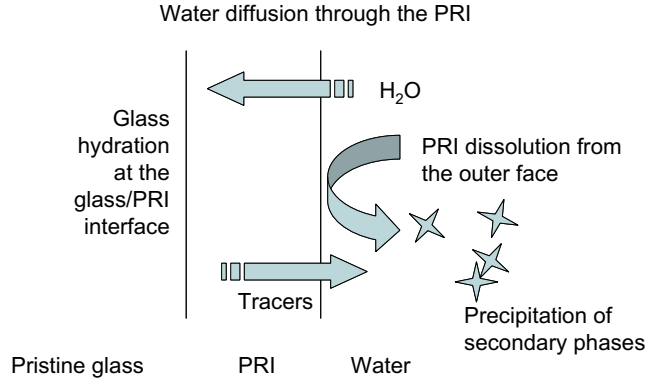

Fig. 1. Simplified diagram of the predominant mechanisms of nuclear borosilicate glass alteration taken into account in the GRAAL model.

Table 1
SON68 glass composition in oxide wt%.

Oxide	wt%	Oxide	wt%	Oxide	wt%
SiO_2	45.85	MoO_3	1.78	CdO	0.03
Al_2O_3	5.00	Cs_2O	1.12	SnO_2	0.02
B_2O_3	14.14	NiO	0.43	TeO_2	0.23
Na_2O	10.22	P_2O_5	0.29	BaO	0.62
CaO	4.07	SrO	0.35	La_2O_3	0.93
Li_2O	1.99	Cr_2O_3	0.53	Ce_2O_3	0.97
ZnO	2.53	Y_2O_3	0.20	Pr_2O_3	0.46
ZrO_2	2.75	MnO_2	0.39	Nd_2O_3	2.04
Fe_2O_3	3.03	Ag_2O	0.03		

2. The analytical GRAAL model

The analytical GRAAL model simplifies the description of nuclear borosilicate glass alteration by assuming the predominance of only two elements: silicon describing the glass matrix evolution, and boron as a mobile element. The equations in this model were given in [8] for glass alteration in a homogeneous medium. The five basic equations describe:

(1) the PRI dissolution kinetics,
(2) the PRI formation kinetics,
(3) the neoformed phase precipitation kinetics,
(4) the silicon mass balance, and
(5) the boron mass balance.

The following nomenclature lists the parameters used in these equations.

2.1. Nomenclature for nuclear glass alteration in a homogenized aqueous solution

- *Observable quantities*
  - $e(t)$, m: PRI thickness at time t
  - $E(t)$, m: dissolved PRI thickness at time t
  - $E_{tot}(t) = E(t) + e(t)$, m: total altered glass thickness at time t
  - $C_{Si}(t)$, mol m^{-3}: silicon concentration in the aqueous solution at time t
  - $C_B(t)$, mol m^{-3}: boron concentration in the aqueous solution at time t
  - $M_{pr}(t)$, mol: quantity of precipitated silica at time t
- *Leaching and operational conditions*
  - S, m^2: reactive surface area of the glass
  - Ω, m^3: reactor volume
  - Q, m s^{-1}: solution volume flow rate
  - M_{init}, kg: initial glass mass
- *Intrinsic glass parameters*
  - C_{vSi}, mol m^{-3}: silicon content in the glass
  - C_{vB}, mol m^{-3}: boron content in the glass
  - ρ_{glass}, kg m^{-3}: glass density
- *Model parameters*
  - C_{sat}, mol m^{-3}: silicon concentration at saturation in equilibrium relation between PRI and aqueous solution. The effect of silicon speciation is not described here
  - C'_{sat}, mol m^{-3}: silicon concentration at the onset of precipitation
  - r_{hydr}, m s^{-1}: hydrolysis rate of soluble glass constituents (boron, alkalis) during creation of the PRI
  - r_{disso}, m s^{-1}: PRI dissolution rate in pure water
  - D_{PRI}, m^2 s^{-1}: water diffusion coefficient in PRI
  - k', m s^{-1}: precipitation rate parameter for secondary silica phases
  - S', m^2: surface area on which secondary phases precipitate
  - ρ', mol m^{-3}: silica density of secondary phases

Note: only a single type of secondary phase is considered here.

2.2. Analytical GRAAL model equations in a homogenized aqueous solution

The equations from [8] are included below with a brief description of the modeled mechanism.

2.2.1. Eq. (1): Dissolution of the passivating reactive interphase

The PRI is assumed to dissolve as a result of the affinity of silicon (Eq. (1)), where r_{disso} corresponds to the PRI dissolution rate and C_{sat} to the total silicon concentration at which dissolution ceases:

$$\frac{dE}{dt} = r_{disso}\left(1 - \frac{C_{Si}(t)}{C_{sat}}\right) \tag{1}$$

2.2.2. Eq. (2): Formation of the passivating reactive interphase

The PRI is assumed to form by water diffusion at the interface with the pristine glass, which hydrolyzes the most soluble glass elements, especially boron. The diffusion coefficient D_{PRI} is about 10^{-22} m^2 s^{-1} for the SON68 glass. Moreover, hydrolysis of the B–O–Si bonds is theoretically limited by kinetics expressed as a rate, r_{hydr}. This gives the following equation, in which the water diffusion profile in the PRI is assumed linear in the interval $[E(t), E(t) + e(t)]$:

$$\frac{de}{dt} = \frac{r_{hydr}}{1 + \frac{e r_{hydr}}{D_{PRI}}} - \frac{dE}{dt} \tag{2}$$

2.2.3. Eq. (3): Secondary phase precipitation kinetics

In the analytical GRAAL model, secondary phase precipitation concerns only silicon by a sink term; it is assumed that only a single phase is formed. The precipitate mass formed over time is assumed in this model to follow an affine relationship described by the following equation, in which the rate term k' is applicable to a precipitation surface area S' for a precipitate of density ρ', which precipitates as soon as the total silicon concentration is above a threshold concentration C'_{sat}:

$$\frac{dM_{pr}}{dt} = \rho' k' S' \left(\frac{C_{Si}(t)}{C'_{sat}} - 1\right) \tag{3}$$

Note that Eq. (3) differs from the equation proposed in [8] using a linear term, without threshold. An affine first-order law is more realistic, corresponding to a precipitation kinetics driven by sursaturation, which application to silica precipitation is given in [17]. This equation is algebraic, in the sense that the neoformed precipitates redissolve as soon as the silicon concentration $C_{Si}(t)$ is less than C'_{sat}. However, redissolution occurs under the condition that the total mass of precipitate $\boldsymbol{M}_{pr}(\boldsymbol{t})$ remains positive:

$$\text{If } M_{pr}(t) = 0 \quad \text{and} \quad C_{Si}(t) < C'_{sat}, \quad \text{then} \quad \frac{dM_{pr}}{dt} = 0 \tag{4}$$

2.2.4. Eq. (4): silicon balance

The silicon concentration variation in the reactor volume, Ω , is determined by the algebraic sum of the following three terms:

- the silicon contribution (source term) due to dissolution of the PRI, with a surface area S and a silicon mass concentration equal to C_{vSi}
- the sink term corresponding to the mass of silicon precipitated in the reactor, given by Eq. (3)
- the sink term due to silicon removal by the volume flow rate Q

This gives the following equation:

$$\Omega \frac{dC_{Si}}{dt} = S C_{vSi} \frac{dE}{dt} - Q C_{Si}(t) - \frac{dM_{pr}}{dt} \tag{5}$$

2.2.5. Eq. (5): boron balance

The boron balance (boron is an overall glass alteration tracer) is obtained in a similar manner to the silicon balance, except that boron does not precipitate and the source term is specified from the total quantity of altered glass, $E(t) + e(t)$:

$$\Omega \frac{dC_B}{dt} = S C_{vB} \frac{d(E+e)}{dt} - Q C_B(t) \tag{6}$$

2.2.6. Initial conditions

Inasmuch as Eqs. (1)–(6) describe the alteration of a pristine SON68 glass sample in initially pure water, the following initial conditions were selected for the remainder of this study:

$$E(0) = 0 \quad (7)$$
$$e(0) = 0 \quad (8)$$
$$M_{pr}(0) = 0 \quad (9)$$
$$C_{Si}(0) = 0 \quad (10)$$
$$C_B(0) = 0 \quad (11)$$

Although the GRAAL model could describe other boundary conditions, we chose to limit the scope to these values because most laboratory experiments relevant to this model concern pristine glass samples in initially pure water.

2.3. Analytical GRAAL model parameter values for SON68 glass

The parameter values for the analytical GRAAL model were determined from physical and chemical considerations and on the basis of a few experimental comparisons. They are indicated here for SON68 glass for leaching in initially pure water at 90 °C. Under these conditions, the progressive enrichment of the aqueous solution results in an increase in the pH toward slightly basic values (between 8 and 9.5 depending on the conditions). Strictly speaking, the effect of the pH on the model parameters should be taken into account since even though the pH quickly reaches an equilibrium level, its value depends on the test conditions. In the analytical GRAAL model, however, this effect is not taken into account because it does not radically modify the parameter values, and in particular those describing the residual kinetics, and because allowing for this effect would entail additional complexity.

The parameter values for the model are the following:

- $C_{sat} = 2.0$ mol m^{-3}: This parameter is interpreted as the PRI solubility limit. Its value is determined by the silica concentration limit in the reactor for dynamic tests at low flow rates per unit area (Q/S) or for tests under static conditions. In the analytical GRAAL model, this represents the solubility limit for total silicon and not for H_4SiO_4 as in the geochemical GRAAL model [9].
- $C'_{sat} = 1.9$ mol m^{-3} is the secondary phase solubility limit. Since the analytical GRAAL model simplifies the chemistry such that the precipitates are reduced to one single phase, and the secondary phase precipitation is the sole mechanism capable of accounting for long term constant (or nondecreasing) rates under static conditions, the C'_{sat} value must be less than C_{sat}. This is a preliminary value; more thorough experimental fitting would be necessary to determine an accurate value. This issue is discussed in the context of the sensitivity calculations.
- $r_{hydr} = 1 \times 10^{-11}$ m s^{-1} is always interpreted as the kinetic parameter of the pristine glass to hydrated glass conversion reaction at the PRI internal interface. The hydration kinetics parameter r_{hydr}, must be distinguished from the initial glass alteration rate measured in pure water (generally designated r_0). r_{hydr} corresponds to the upper limit of the tracer release rate, which otherwise would initially be infinite because the release follows a diffusion process. The rationale for an upper limit lies in the reactive nature of this diffusion [18]. No maximal value can be inferred from the state-of-the-art knowledge. Therefore, a reference value of 10^{-11} m s^{-1} is selected, so that the forward initial rate is not limited by this hydration phenomenon. It will be shown below that the value of r_{hydr} has negligible impact on the predictions of the model.
- $r_{disso} = 1.7 \times 10^{-12}$ m s^{-1}: This is the kinetic parameter for the PRI dissolution rate on the outer face. According to the GRAAL model, r_{disso} is the asymptotic rate of release of tracer elements and silica during experiments at high solution renewal rates. It is also the initial silica release rate (but not that of the tracers, at least during the initial instants of alteration); r_{disso} is therefore assigned both by silica concentration measurements in the reactor for tests at high Q/S ratios, and by equilibrium rate measurements for tests at high Q/S values (for which this rate is dominated by the PRI dissolution kinetics). The proposed value corresponds to the initial rate values (r_0) measured at 90 °C and neutral pH (0.15 μm d^{-1}) [12,19].
- $D_{PRI} = 3 \times 10^{-22}$ m^2 s^{-1} is the constant for water diffusion in the PRI. Its value can be fitted on the boron concentration peak values obtained during tests at low flow rate. This value is within the range Chave et al. determined by analyzing boron profiles in the PRI [20].
- $k' = 2 \times 10^{-14}$ m s^{-1} and $S' = S$: Secondary phase precipitation is expressed as the product of the kinetic term k' by the precipitate surface area S'. In the analytical GRAAL model compared with glass leach tests in homogeneous media, the product $k'S'$ can be determined (with an uncertainty higher than an order of magnitude) by the residual rate value for the static tests or dynamic tests at low flow rates (for which the residual rate is dominated by the secondary phase precipitation kinetics). Moreover, alteration tests performed at various S/V values showed that the residual rate was relatively independent of the glass surface area S [21,22]. In such conditions, the product $k'S'$ can be considered as proportional to $r_{res}S$ (Eq. (5) applied to a zero flow rate and a stationary concentration), r_{res} being the apparent glass alteration residual rate measured in the static experiments and shown to be independent of the glass surface area. Since the S'/S ratio can be incorporated in the value of k', this is equivalent to considering that S' is equal to S. In other words, one can infer from the observations of long-term alteration rates for nuclear borosilicate glasses under static conditions, that the secondary phase precipitation mechanism, in terms of explaining the observed glass behaviour, needs only the determination of the product $k'S'$ and does not need to discriminate between both terms. In this scope, a precipitate with low surface area and high precipitation rate is isomorphic to a precipitate with high surface area and low precipitation rate. However, if additional precipitation were taken into account far from the glass, in a surrounding medium with known precipitate surface area, such as an engineered or geological barrier (see Section 4.1.3), then the individual value of k' would matter again.
- $\rho' = 2 \times 10^4$ mol m^{-3} corresponds to a silica content in the precipitate comparable to its concentration in SON68 glass; this is a reasonable order-of-magnitude hypothesis corresponding to the values found in neoformed phases in contact with clay [9,23]. In any event, this parameter affects only the product $\rho'k'S'$, and the uncertainty on this product is dominated by k'.

Finally, the intrinsic parameters of SON68 glass—its silicon and boron content—are respectively equal to $C_{vSi} = 2.07 \times 10^4$ mol m^{-3} and $C_{vB} = 1.10 \times 10^4$ mol m^{-3} [9,22].

All the input parameters of the analytical GRAAL model are summarized in Table 2, which indicates the reference value together with the minimum and maximum values used in the sensitivity study for each parameter. The choice for the latter values is discussed in this study (Section 3.3), within the subsections pertaining to the relevant parameters (Section 3.3.1, 3.3.2, 3.3.3, 3.3.4, 3.3.5).

2.4. Solution of analytical GRAAL model equations: Main characteristic quantities

Eqs. (1)–(6), with initial conditions (7)–(11), can be solved purely analytically for the silicon concentrations, the dissolved PRI thickness ($E(t)$), and the precipitate mass. The boron concentrations

Table 2
Analytical GRAAL model input parameter values for SON68 glass altered in initially pure water.

Parameter	Notation/unit	Reference	Min.	Max.
Total Si concentration at saturation	C_{sat} (mol m^{-3})	2.0	1.0	4.0
Si precipitation threshold	C'_{sat} (mol m^{-3})	1.9	0.95[a]	3.8[a]
Rate of pristine glass hydration forming the PRI	r_{hydr} (m s^{-1})	10^{-11}	3×10^{-12}	10^{-7}
PRI dissolution rate	r_{disso} (m s^{-1})	1.7×10^{-12}	1.0×10^{-12}	9.0×10^{-12}
Diffusion coefficient in the PRI	D_{PRI} (m^2 s^{-1})	3×10^{-22}	6×10^{-23}	6×10^{-22}
Neoformed phase precipitation rate	k' (m s^{-1})	2×10^{-14}	5×10^{-15}	10^{-13}
Precipitation to glass surface area ratio	S'/S	1	–	–
Si content of neoformed phases	ρ' (mol m^{-3})	2×10^4	–	–
Si content of SON68 glass	C_{vSi} (mol m^{-3})	2.07×10^4	–	–
B content of SON68 glass	C_{vB} (mol m^{-3})	1.10×10^4	–	–
Density of SON68 glass	ρ_{glass} (kg m^{-3})	2.74×10^3	–	–

[a] When the C'_{sat} concentration is modified proportionally to C_{sat}.

and PRI thicknesses ($e(t)$) are calculated numerically using a Fortran program based on Eulerian stepwise calculations, or from semi-analytical approximations. The complete equation system is indicated in Appendix A; its solution reveals the main characteristic quantities of the model (Appendix A.2). These characteristic quantities are used to develop the analytical or semi-analytical expressions for the concentrations, alteration rates, and total altered thickness in Appendix A.3.

The characteristic time values are indicated in Table 3; the units are specified in the nomenclature of Section 2.1. Using the model parameters defined in Section 2.3, numerical values are proposed according to the S/V ratio (designated here S/Ω) and the flow rate per unit area (Q/S), expressed in SI units (time in seconds, S/Ω in m^{-1} and Q/S in m s^{-1}).

The existence of a precipitation threshold in Eq. (3), results in two successive glass alteration regimes: before and after the beginning of precipitation, if it occurs—which requires that the equilibrium silicon concentration without precipitation (C_{sat1}, see Table 3) be higher than the precipitation threshold C'_{sat}. This can be expected under static conditions or for sufficiently low flow rates per unit area (Q/S), below 10^{-9} m s^{-1} using the model parameter values specified in Section 2.3. Each regime defines two characteristic time values, one for silicon concentration variations (t_{c1} and t_{c2}), and the other for the evolution of the PRI and thus the boron concentrations (t_{PRI1} and t_{PRI2}). The values of t_{c1} and t_{c2} are generally a few days except at very low S/V ratios (designated here S/Ω), whereas t_{PRI1} and t_{PRI2} can be very high at very low flow rates per unit area. Under static conditions, t_{PRI1} is infinite (the PRI grows according to an asymptotic square-root-of-time relation $t^{1/2}$ without precipitation), and t_{PRI2} is determined by the effect of precipitation (about 9 years).

Finally, precipitation of a silicated secondary phase implies the existence of a nonzero asymptotic residual glass alteration rate, r_f, i.e. congruent alteration at a rate given by the following expressions:

$$r_f = r_{f1} = r_{disso}\left(1 - \frac{C_{sat1}}{C_{sat}}\right) = r_{disso}\frac{QC_{sat}}{SC_{vSi}r_{disso} + QC_{sat}} = \frac{1}{\frac{SC_{vSi}}{QC_{sat}} + \frac{1}{r_{disso}}} \quad (12)$$

Table 3
Characteristic time values of analytical GRAAL model. The numerical values given in this table are based on the reference parameter values from Table 1 (Section 2.3).

Characteristic time/quantity	Definition
$t_{kin} = \frac{\Omega C_{sat}}{SC_{vSi}r_{disso}} = (5.7 \times 10^7 \text{ s m}^{-1})\frac{\Omega}{S}$	Characteristic time for solution saturation under static conditions, neglecting precipitation
$t_{reac} = \frac{\Omega}{Q}$	Characteristic residence time of inert elements in the reactor, taking the flow rate into account
$t_{prec} = \frac{\Omega C'_{sat}}{\rho' k' S'} = (4.8 \times 10^9 \text{ s m}^{-1})\frac{\Omega}{S}$	Characteristic time for precipitation of silicon in the reactor
t_{c1} given by : $\frac{1}{t_{c1}} = \frac{1}{t_{kin}} + \frac{1}{t_{reac}}$	Characteristic time for the evolution of the silica concentration in the system in the absence of precipitation, taking into account the silica saturation and the flow rate
t_{c2} given by: $\frac{1}{t_{c2}} = \frac{1}{t_{kin}} + \frac{1}{t_{reac}} + \frac{1}{t_{prec}}$	Characteristic time for the evolution of the silica concentration in the system after the onset of precipitation, taking into account the silica saturation and the flow rate
$C_{sat1} = C_{sat}\frac{t_{c1}}{t_{kin}} = \frac{C_{sat}}{1 + (5.7 \times 10^7 \text{ s m}^{-1})Q/S}$	Steady-state silica concentration in the reactor in the absence of precipitation, taking into account the effect of the flow rate
$t_{opr} = -t_{c1}\ln\left(1 - \frac{C'_{sat}}{C_{sat1}}\right)$	Time to the onset of precipitation, if precipitation occurs, assuming $C'_{sat} < C_{sat1}$ (thus, $Q/S < 9.2 \times 10^{-10}$ m s^{-1})
$t_{PRI1} = \frac{D_{PRI}}{r_{disso}^2}\left(1 + \frac{SC_{vSi}r_{disso}}{QC_{sat}}\right)^2 = (10^2 \text{ s})\left(1 + (1.75 \times 10^{-8} \text{ m s}^{-1})S/Q\right)^2$	Characteristic time for formation of the PRI in the absence of precipitation
$t_{PRI2} = \frac{D_{PRI}}{r_{disso}^2}\left(1 + \frac{SC_{vSi}r_{disso} + \rho' k' S'}{QC_{sat}} + \rho' k' S'\left(\frac{C_{sat}}{C'_{sat}} - 1\right)\right)^2$	Characteristic time for formation of the PRI in the presence of precipitation

if the flow rate is sufficient that the asymptotic concentration C_{sat1} does not exceed the precipitation threshold C'_{sat},

$$r_f = r_{f2} = r_{disso}\frac{QC_{sat} + \rho' k' S'\left(\frac{C_{sat}}{C'_{sat}} - 1\right)}{SC_{vSi}r_{disso} + QC_{sat} + \rho' k' S'\frac{C_{sat}}{C'_{sat}}} \approx \frac{Q}{S}\frac{C_{sat}}{C_{vSi}} + \frac{\rho'}{C_{vSi}}\frac{S'}{S}k'\left(\frac{C_{sat}}{C'_{sat}} - 1\right) \quad (13)$$

if the flow rate is low enough for precipitation to occur ($C_{sat1} > C'_{sat}$). There will therefore always be a minimal alteration rate—about 10^{-15} m s^{-1} at 90 °C—at very low flow rates. Such rate is three orders of magnitude lower than r_{disso} and nearly four orders of magnitude lower than the forward dissolution rate for SON68 at 90 °C and

pH 9. At higher flow rates per unit area, Q/S the alteration rate is roughly proportional to the Q/S ratio. Finally, at very high flow rates per unit area, i.e. when $\frac{Q}{S}\frac{C_{sat}}{C_{vSi}}$ is of the order of magnitude of r_{disso}, the residual rate becomes independent of Q/S, and approaches r_{disso}.

Under these steady-state conditions the PRI thickness is then equal to $\lambda_{PRI} = D_{PRI}/r_f$, or about 300 nm for the minimum value of r_f (10^{-15} m s^{-1}), and the formation of the PRI will continue under steady-state conditions for a time exceeding $t_{PRI} = D_{PRI}/r_f^2$: about 10 years if r_f is equal to 10^{-15} m s^{-1}, i.e. longer than the time necessary to reach a steady-state silicon concentration. In other words, in this time period alteration will not be congruent because of the time required to reach a steady-state boron concentration.

Applying the analytical GRAAL model to leach tests on initially pristine glass in initially pure homogenized water will therefore always give a rising silicon concentration curve because of the expression for the precipitation kinetics versus the concentrations. This not only excludes the possibility of a resumption of alteration (which would require a decrease in the silicon concentration at the PRI/solution interface) but also any redissolution of the precipitate. With these hypotheses it is therefore impossible to reproduce the observed resumption of alteration [24,25]. However, these phenomena occurred at very high pH (greater than 10) which are not observed for R7T7-type glass and are outside the validity range of the analytical GRAAL model, which assumes a constant concentration at saturation (C_{sat}). Conversely, the geochemical GRAAL model, which allows for the precipitation of a number of phases, could account for such phenomena.

3. Comparing the analytical GRAAL model with laboratory alteration tests on SON68 glass

3.1. List of tests

The predictions of the analytical GRAAL model can be compared with the results of SON68 glass laboratory alteration tests at 90 °C in initially pure water under static or dynamic conditions at different S/V ratios and different flow rates per unit area, Q/S. Two series of tests were selected for comparison:

- 12 tests under static conditions or at low flow rate per unit area, which were compared with the results predicted by the geochemical GRAAL model in [9]. These tests are listed in Table 4; the experimental details are discussed in [9].
- 19 other tests at moderate flow rates per unit area, listed in Table 5.

3.2. General comparison of test results with analytical GRAAL model predictions

The comparison concerns the evolution of the silicon and boron concentrations. The total altered glass mass can be computed from the boron concentration. The model predictions and experimental findings are compared in Fig. 2, where the mass calculated from measured values is plotted along the X-axis and the mass predicted by the analytical GRAAL model on the Y-axis. Two series of points

Table 4
Static and low flow rate experiments performed on SON68 glass at 90 °C, from [9].

Exp^t	Duration (days)	S/V (cm^{-1})	Q/S (m s^{-1})	Powder size (μm)	BET specific surface area (m^2 g^{-1})	Powder mass (g)	Initial pure water volume (mL)
1	550	3.3	0	63–125	0.052	1.6	250
2	2800	80	0	40–100	0.097	25	300
3	110	200	0	Centered around 1.5	4.5	0.67	150
4	3000	2000	0	5 à 40	0.58	52	150
5	59	4700	1.7×10^{-12}	Centered around 1.5	4.5	30	290
6	59	2100	6.6×10^{-12}	Centered around 1.5	4.5	8.0	170
7	90	4600	1.5×10^{-11}	Centered around 5	1.4	100	300
8	70	1200	4.4×10^{-11}	Centered around 5	1.4	25	300
9	91	820	1.5×10^{-10}	Centered around 5	1.4	10	170
10	70	100	5.7×10^{-10}	Centered around 5	1.4	2.5	350
11	90	85	1.5×10^{-9}	Centered around 5	1.4	1.0	170
12	70	28	5.9×10^{-9}	Centered around 5	1.4	0.25	120

Table 5
List of moderate flow rate experiments performed on SON68 glass at 90 °C.

Exp^t	Duration (days)	S/V (cm^{-1})	Q/S (m s^{-1})	Powder size (μm)	Specific/BET surface area (m^2 g^{-1})	Powder or coupon mass (g)	Initial pure water volume (mL)	Reference
13	16	9.7	6.9×10^{-9}	100–125	4.2×10^{-2}	2.6	110	[26]
14	16	9.7	6.9×10^{-9}	100–125	4.2×10^{-2}	2.6	110	[26]
15	7.9	9.7	1.2×10^{-8}	100–125	4.2×10^{-2}	2.6	110	[26]
16	40	9.7	1.2×10^{-8}	100–125	4.2×10^{-2}	2.6	110	[26]
17	40	9.7	1.6×10^{-8}	100–125	4.2×10^{-2}	2.6	110	[26]
18	40	9.7	3.3×10^{-8}	100–125	4.2×10^{-2}	2.6	110	[26]
19	40	9.7	4.7×10^{-8}	100–125	4.2×10^{-2}	2.6	110	[26]
20	12	9.7	1.1×10^{-7}	100–125	4.2×10^{-2}	2.6	110	[26]
21	12	9.7	1.1×10^{-7}	100–125	4.2×10^{-2}	2.6	110	[26]
22	310	220	5.2×10^{-10}	2	4.5	5.0	1000	[27]
23	310	70	1.7×10^{-9}	5	1.4	5.0	1000	[27]
24	310	29	3.9×10^{-9}	12	5.8×10^{-1}	5.0	1000	[27]
25	310	15	7.2×10^{-9}	20	2.9×10^{-1}	5.0	1000	[27]
26	60	0.47	1.2×10^{-8}	Coupon	4.1×10^{-4}	14	120	[27]
27	60	0.47	5.0×10^{-8}	Coupon	4.1×10^{-4}	14	120	[27]
28	60	0.47	6.9×10^{-8}	Coupon	4.1×10^{-4}	14	120	[27]
29	60	0.47	1.2×10^{-7}	Coupon	4.1×10^{-4}	14	120	[27]
30	130	0.61	1.6×10^{-8}	Coupon	6.3×10^{-5}	680	700	[28]
31	110	0.61	3.0×10^{-8}	Coupon	6.9×10^{-5}	680	770	[28]

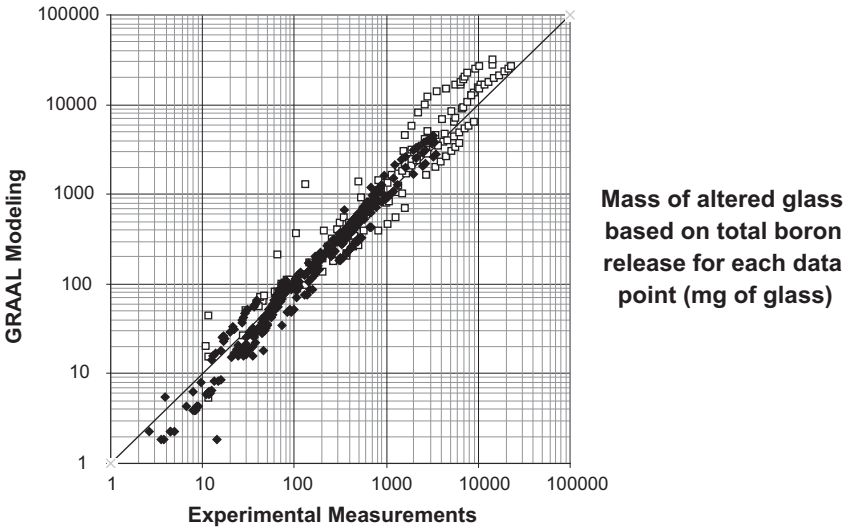

Fig. 2. Comparison of the experimental and predicted (analytical GRAAL model) altered glass masses for all data with an altered glass fraction less than 70%. White squares correspond to static and low flow rate experiments used in [9] (Table 4), and black diamonds correspond to additional moderate flow rates experiments (Table 5).

are shown, corresponding to tests under static or low flow rate conditions (Table 4), and tests at moderate flow rates (Table 5). All the experimental data points in each test are compared, except for those corresponding to a high altered glass fraction (>70%) since the latter cannot be corrected to the shrinking core effect and therefore may alter the interpretations.

The overall comparison appears to be satisfactory, and the difference between the predicted and measured altered glass mass is less than a factor of 3. More precisely, the root mean square deviation from zero, calculated from the quantity $\log_{10}(M_{exp}/M_{calc})$, is equal to 0.185 for all the tests, to 0.248 for the tests 1–12 (static and low flow rate) and to 0.148 for the tests 19–31 (moderate flow rate). The overall statistics show a deviation between experimental and predicted values lower than a factor 2 for 92% of all points, and lower than a factor 1.5 for 71% of all points. This is a good result considering the large number of experimental data reproduced using a single set of input parameters—particularly since the model is based on simplified hypotheses concerning the nature of the passivating barrier: it is reduced to the action of the PRI, without allowing for diffusion barrier effect of the rest of the alteration gel, which also contributes to diminishing the glass alteration rate. As this effect becomes increasingly prominent as the thicknesses of the alteration gel increases, GRAAL can be expected to overestimate the altered glass mass with thicker gels. This is apparent in Fig. 2, regardless of the flow rate.

Another area of agreement between the analytical GRAAL model and the experimental findings is found for flowing tests by comparing the predicted and measured steady-state silicon concentrations, i.e. over time periods much longer than t_{c1} (without precipitation) or t_{c2} (with precipitation), as in Fig. 3. It is to be noted however that this figure shows an agreement on the trends but not in all detail. The disagreements is due to the choice of a unique value for C_{sat} (total Si concentration at saturation) in the analytical GRAAL model, without taking into account silicon speciation in solution. If the latter is taken into account, the equilibrium pH and thus C_{sat}, is expected to depend on the flow rate and have higher values for lower flow rates. This corresponds to the experimental values on Fig. 3. However, taking into account this approximation, the model-experiment comparison can still be considered as satisfactory over a range of flow rates per unit area spanning more than four orders of magnitude.

The residual alteration rates are also compared for flowing tests in Fig. 4. Once again, the result is satisfactory. However, this figure displays a predicted boron release rate near 6×10^{-15} m s^{-1} for very low flow rates, a factor 6 above the residual alteration rate due to precipitation (1.0×10^{-15} m s^{-1}). That can be explained by the durations of these tests (experiments 5 and 6), much shorter (60 days) than the equilibrium time of the PRI under such conditions (10 years for $D_{PRI} = 3 \times 10^{-22}$ m^2 s^{-1} and $r_f = 10^{-15}$ m s^{-1}). Therefore, the PRI has not yet reached its equilibrium thickness, though the system is in equilibrium regarding silicon. If this effect is taken into account, as well as the choice of r_{disso} as the forward

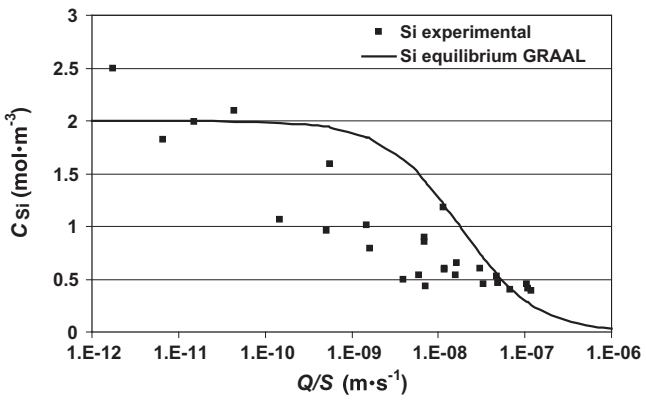

Fig. 3. Comparison of the experimental and predicted silicon concentrations at steady-state (C_{Si}), versus the flow rate (Q/S), for nonstatic experiments.

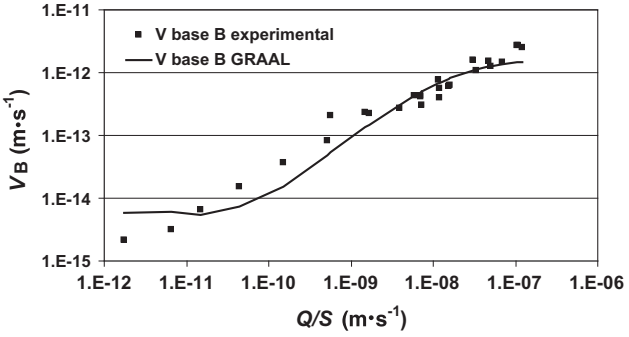

Fig. 4. Comparison of the experimental and predicted alteration rates with respect to boron (V_B), versus the flow rate (Q/S), for nonstatic experiments.

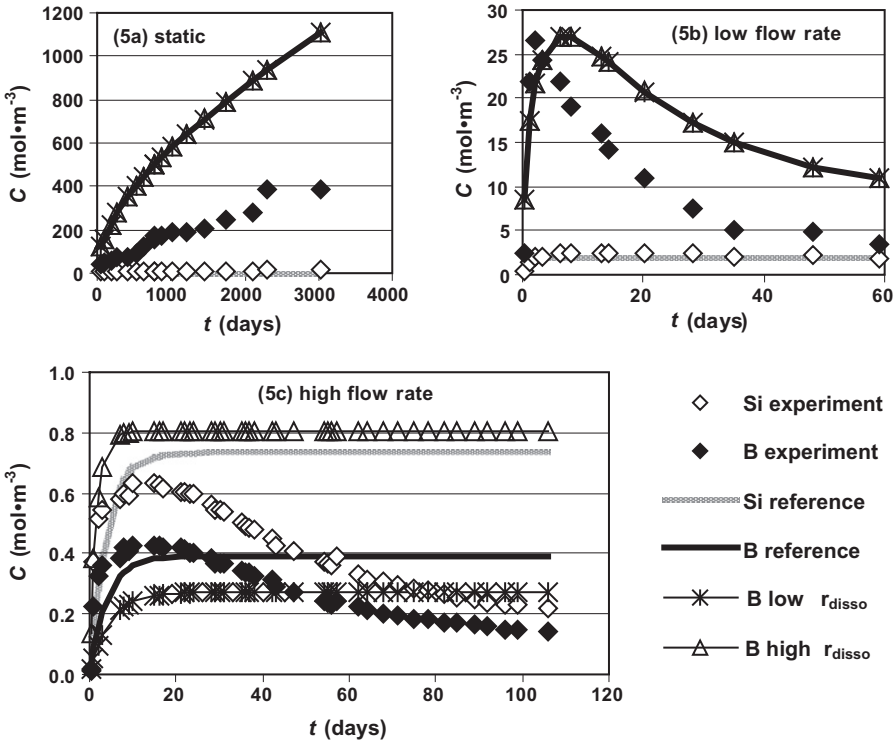

Fig. 5. Sensitivity of analytical GRAAL model predictions versus r_{disso} parameter (PRI dissolution rate) – Comparison with static (a, Exp. 4, 2000 cm^{-1}), low flow rate (b, Exp. 6, 2100 cm^{-1}, $Q/S = 6.6 \times 10^{-12}$ m s^{-1}), and high flow rate (c, Exp. 31, 0.61 cm^{-1}, $Q/S = 3.0 \times 10^{-8}$ m s^{-1}) tests. The reference, low and high value for r_{disso} are respectively 1.7×10^{-12} , 1.0×10^{-12} and 9.0×10^{-12} m s^{-1}.

dissolution rate in pure water at pH 7, one can explain why the predicted rates displayed in Fig. 4 do not exceed a factor 300 between the highest and the lowest flow rates. On the other hand, at pH 9–9.5 (pH range observed under stationary conditions at low flow rates for SON68 glass alteration), the ratio of the initial to the final rates is around 10^4.

3.3. Sensitivity study by comparison with selected tests

The objective of this study is to identify the sensitivity of certain model input parameter by examining a few characteristic tests:

- Test 4, under static conditions at 2000 cm^{-1}.
- Test 6, at a low flow rate ($Q/S = 6.6 \times 10^{-12}$ m s^{-1}) and a high S/V ratio (2100 cm^{-1}).
- Test 31, at a high flow rate ($Q/S = 3.0 \times 10^{-8}$ m s^{-1}) and low S/V ratio (0.61 cm^{-1}).

This sensitivity study is designed to evaluate the robustness of the model parameters with regard to the available experimental data. This is done using comparisons with experiments in trend but not necessarily in all details, due to the nature of the approximations made in the GRAAL model and especially in its analytical implementation: PRI described as an homogeneous diffusive layer, external gel layer not taken into account, solution chemistry based solely on silicon neglecting moreover the effects of pH, precipitation of a single neoformed phase.

The sensitivity study concerns each of the major parameter of the analytical GRAAL model:

- the PRI dissolution rate, r_{disso};
- the glass network hydration rate, r_{hydr};
- the diffusion coefficient of water and the mobile elements in the PRI, D_{PRI};
- the Si concentration at saturation, C_{sat}; and
- the precipitation law, represented by k' (precipitation kinetics parameter).

The study was performed using the basic values of the model parameters. Each of them was tested between a minimum and maximum value, the choice of which is discussed within the respective section (3.3.1, 3.3.2, 3.3.3, 3.3.4, 3.3.5) with all other parameter values held constant. This, with the exception of the sensitivity of C_{sat}, for which the C'_{sat} parameter (precipitation threshold) was modified proportionally; in other words, in this case the precipitation kinetics were assumed to remain constant near C_{sat}.

The minimum, maximum and reference values for each parameter are listed in Table 2 (Section 2.3).

3.3.1. Sensitivity to the PRI dissolution rate (r_{disso})

The model sensitivity to r_{disso} was tested for a maximum PRI dissolution rate of 9×10^{-12} m s^{-1} corresponding to a value near r_{hydr} (set constant at 10^{-11} m s^{-1} in the exercise) and not far from the initial dissolution rate of SON68 glass (r_0) experimentally measured at pH 9 in Ref. [19]. The minimum value of 1×10^{-12} m s^{-1} for r_{disso} corresponds to the lower bound on r_0 at neutral pH. The results for experiments under static conditions at high S/V ratio (Experiment 4), under low flow rate (Experiment 6) and under high flow rate (Experiment 31) are shown in Fig. 5 (respectively 5a, b and c).

As expected, a significant difference is observed for the tests at high flow rates. Decreasing the value of r_{disso} appears to account for the smaller quantitative difference with the measured concentrations, at least during the initial phase of rising concentrations. The value of r_{disso} could be more closely fitted on the basis of these comparisons, but this was not the main objective of this study—especially since the detailed evolution of the concentrations, especially the diminishing values observed after the longest time periods, are due to transient phenomena (evolution of a relatively

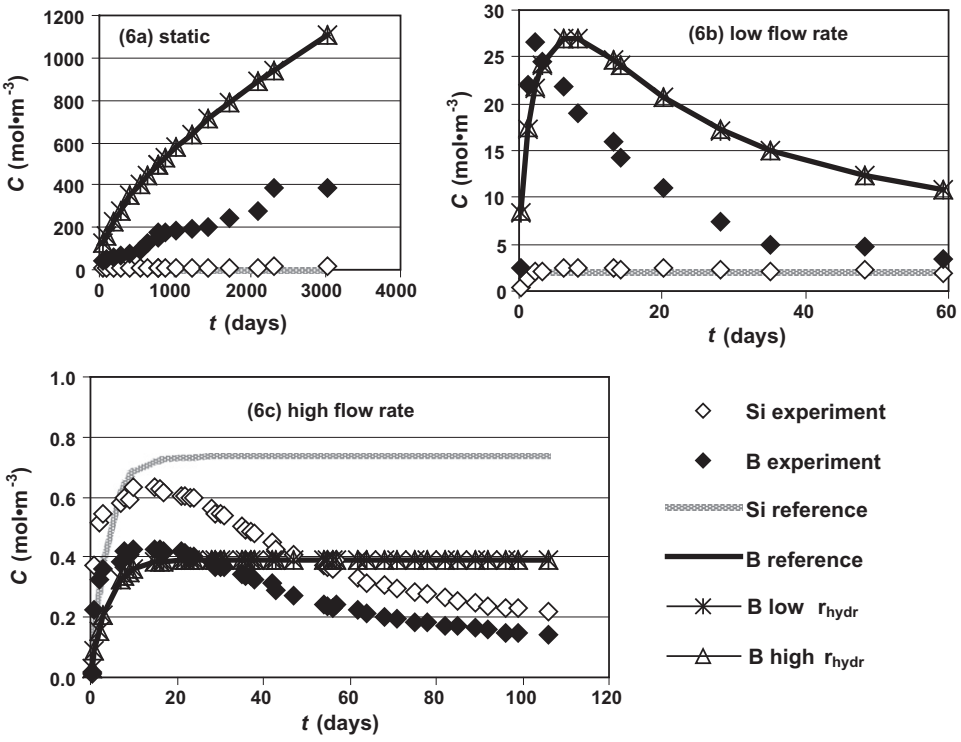

Fig. 6. Sensitivity of analytical GRAAL model predictions versus r_{hydr} parameter (glass hydration rate) – Comparison with static (a, Exp. 4, 2000 cm^{-1}), low flow rate (b, Exp. 6, 2100 cm^{-1}, $Q/S = 6.6 \times 10^{-12}$ m s^{-1}), and high flow rate (c, Exp. 31, 0.61 cm^{-1}, $Q/S = 3.0 \times 10^{-8}$ m s^{-1}) tests. The reference, low and high value for r_{hydr} are respectively 1×10^{-11} , 3×10^{-12} and 1×10^{-7} m s^{-1}.

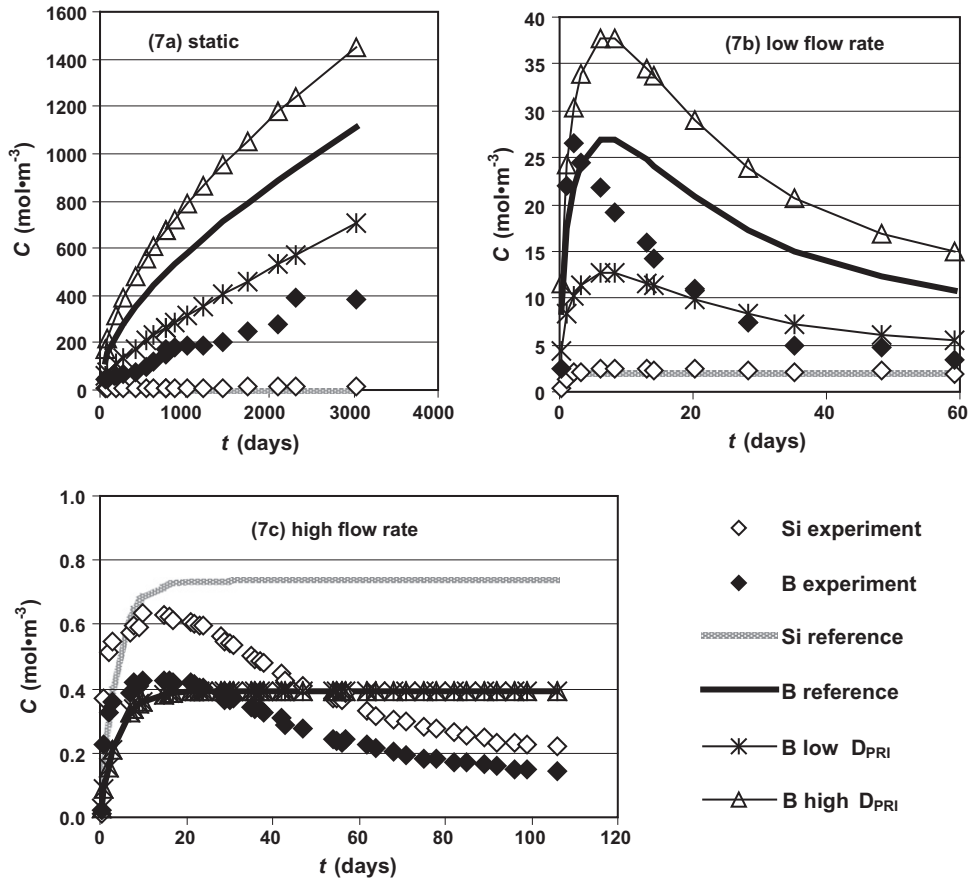

Fig. 7. Sensitivity of analytical GRAAL model predictions versus D_{PRI} parameter (diffusion coefficient of water and mobile elements in the PRI) – Comparison with static (a, Exp. 4, 2000 cm^{-1}), low flow rate (b, Exp. 6, 2100 cm^{-1}, $Q/S = 6.6 \times 10^{-12}$ m s^{-1}), and high flow rate (c, Exp. 31, 0.61 cm^{-1}, $Q/S = 3.0 \times 10^{-8}$ m s^{-1}) tests. The reference, low and high value for D_{PRI} are respectively 3×10^{-22} , 6×10^{-23} and 6×10^{-22} m^2 s^{-1}.

nonprotective gel) that the GRAAL model was not designed to describe in detail.

3.3.2. Sensitivity to the glass hydration rate (r_{hydr})

The sensitivity to r_{hydr} was evaluated for a maximum hydration rate of 10^{-7} m s^{-1} largely exceeding r_{disso}, and a minimum rate of 3×10^{-12} m s^{-1} near r_{disso} ($r_{disso} = 1.7 \times 10^{-12}$ m s^{-1}). The results for the static, low flow rate and high flow rate experiments (4, 6 and 31) are shown in Fig. 6.

In each case (static, low flow rate, and high flow rate), the effect of r_{hydr} is negligible. This is not surprising because the sensitivity of the Si and B concentrations to this parameter concerns an altered thickness of no more than about D_{PRI}/r_{hydr}, or a maximum of 1 angström when $D_{PRI} = 3 \times 10^{-22}$ m^2 s^{-1} and $r_{hydr} = 3 \times 10^{-12}$ m s^{-1}. To obtain a measurable effect within a reasonable time frame would require a high value for D_{PRI} (>10^{-20} m^2 s^{-1}) and a low value for r_{hydr} (near r_{disso}). Of course these considerations do not diminish the importance of this parameter as rate-limiting for the release of the most highly mobile elements, although it would theoretically be more pertinent to use a separate value per element or per class of elements (boron ≠ alkalis). This refinement is not required at this stage of development, however.

3.3.3. Sensitivity to the diffusion coefficient in the PRI (D_{PRI})

The sensitivity to D_{PRI} was evaluated for a minimum value of 6×10^{-23} m^2 s^{-1} and a maximum value of 6×10^{-22} m^2 s^{-1}, corresponding to the expected variation of the diffusion coefficient at 90 °C between pH 7 and 10, based on the values determined by tests at different S/V ratios analyzed by Chave [20]. The results for the static, low flow rate and high flow rate experiments are shown in Fig. 7.

As expected, D_{PRI} has a major impact on the boron concentrations in solution for the tests under static conditions and at low flow rates, but is negligible at high flow rates because glass alteration is controlled by the solution flow rate. However, a comparison between static and low flow rate tests shows that it is difficult to fit the D_{PRI} parameter closely: the experimental boron concentrations were closer to the model predictions with the reference value (3×10^{-22} m^2 s^{-1}) for short time periods, and with the minimum value (6×10^{-23} m^2 s^{-1}) for longer time scales. This difference is probably attributable to the diffusion barrier effect of the relatively nonprotective gel, resulting in less alteration than would be expected from the PRI formation and dissolution mechanisms alone.

3.3.4. Sensitivity to the silicon concentration at saturation (C_{sat})

The sensitivity to C_{sat} was evaluated for a low value of 1 mol L^{-1} (the concentration at saturation for neutral pH at 90 °C) and a high value of 4 mol L^{-1} to allow for the higher pH (about 9.5) likely to occur if the glass composition leads the chemistry of the surrounding media [29]. For both values the precipitation threshold for neoformed phases (C'_{sat}) was fitted proportionally so the precipitation kinetics remained constant at saturation, in order to assess the specific effect of varying C_{sat}: thus $C'_{sat} = 0.95$ mol m^{-3} when $C_{sat} = 1$ mol m^{-3} and $C'_{sat} = 3.8$ mol m^{-3} when $C_{sat} = 4$ mol m^{-3}. The results for the static, low flow rate and high flow rate experiments are shown in Fig. 8.

If the precipitation kinetics are assumed constant at saturation, the impact of C_{sat} is very limited on the boron concentrations under static or low flow rate conditions, when alteration is dominated by precipitation. At higher flow rates, however, the effect of C_{sat} is significant and can be proportional to C_{sat} at intermediate flow rates, low enough for the silicon concentrations to remain near saturation, but high enough so the impact of precipitation is negligible. For high flow rates (experiment 31) the solution is undersaturated with respect to the PRI, and thus the impact of C_{sat} is therefore less significant.

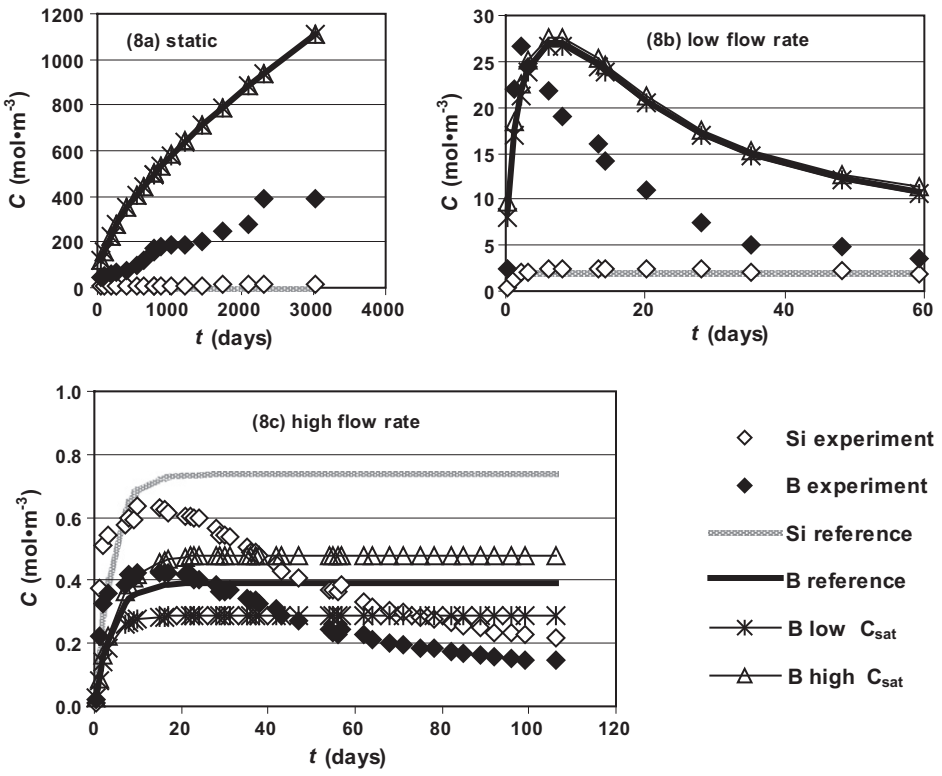

Fig. 8. Sensitivity of analytical GRAAL model predictions versus C_{sat} parameter (total silicon concentration at saturation) with the C'_{sat} parameter (precipitation threshold) fitted proportionally – Comparison with static (a, Exp. 4, 2000 cm^{-1}), low flow rate (b, Exp. 6, 2100 cm^{-1}, $Q/S = 6.6 \times 10^{-12}$ m s^{-1}), and high flow rate (c, Exp. 31, 0.61 cm^{-1}, $Q/S = 3.0 \times 10^{-8}$ m s^{-1}) tests. The reference, low and high value for C_{sat} are respectively 2.0, 1.0 and 4.0 mol m^{-3}.

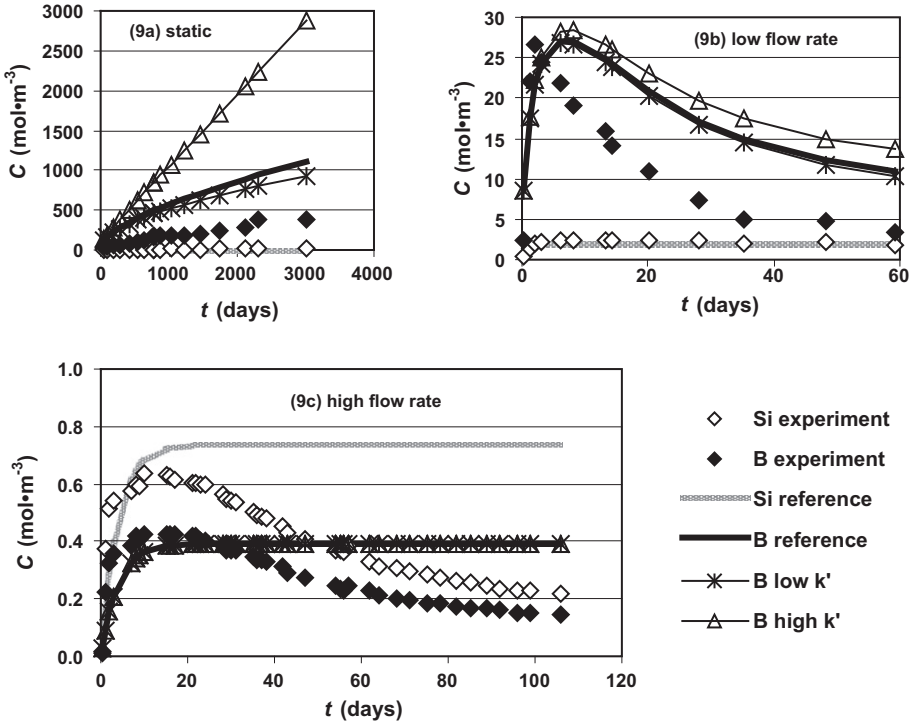

Fig. 9. Sensitivity of analytical GRAAL model predictions versus k' parameter (neoformed phase precipitation kinetics) – Comparison with static (a, Exp. 4, 2000 cm^{-1}), low flow rate (b, Exp. 6, 2100 cm^{-1}, $Q/S = 6.6 \times 10^{-12}$ m s^{-1}), and high flow rate (c, Exp. 31, 0.61 cm^{-1}, $Q/S = 3.0 \times 10^{-8}$ m s^{-1}) tests. The reference, low and high value for k' are respectively 2×10^{-14} , 5×10^{-15} and 1×10^{-13} m s^{-1}.

3.3.5. Sensitivity to precipitation kinetics

The effect of taking precipitation into account was evaluated in terms of the k' parameter, with a minimum value of 5×10^{-15} m s^{-1} and a maximum value of 10^{-13} m s^{-1} corresponding to the uncertainty on the order of magnitude of the phenomenon. The results for the static, low flow rate and high flow rate experiments are shown in Fig. 9.

In all three cases (static, low flow rate, and high flow rate), the difference between the boron concentrations at the reference value of k' (2×10^{-14} m s^{-1}) and at the minimum value, lower by a factor of 4 (5×10^{-15} m s^{-1}) was minimal. The impact on the boron concentration became greater for a high k' value (10^{-13} m s^{-1}), but only for the tests under static conditions (the difference was minor for the low flow rate test). This indicates that there was too much noise in the experimental comparison to discriminate among the various forms or values of precipitation kinetic laws that could have a major long-term impact in a repository.

3.3.6. Discussion and summary

The sensitivity studies identified the parameters affecting glass alteration to varying degrees for laboratory tests. The impact on tests of longer duration, especially under static conditions, is also indicative of the long-term importance of a parameter, even though cumulated short-term effects, such as the pH evolution or the development of an external gel layer, not taken into account in the analytical GRAAL model, could complicate the interpretation of the results and can account for the overestimation of the boron concentrations for the high S/V (2000 cm^{-1}) static test (Exp. 4).

Unsurprisingly, the r_{hydr} and r_{disso} parameters have little impact on alteration (except in the case of r_{disso} for high flow rate tests, which are rather irrelevant for a repository except in certain accident situations). Since the precise value of r_{hydr} is very difficult to obtain experimentally, this very low sensitivity allows to disregard its impact. It is thus sufficient to select a r_{hydr} value high enough with respect to r_{disso} (e.g. 10^{-11} m s^{-1} relatively to 1.7×10^{-12} m s^{-1}).

The value of C_{sat} also has little impact on alteration under static conditions or at low flow rates, at least if the precipitation kinetics are assumed constant at saturation, i.e. if the value of C'_{sat} is fitted proportionally to C_{sat}. This is due to the fact that glass alteration is controlled by precipitation of a silicated secondary phase at sufficiently low flow rates. On the other hand, if C'_{sat} is kept constant (corresponding to a particular secondary phase dominating the precipitation phenomenon), the value of C_{sat} has an important impact, proportionally to the term $C_{sat}/C'_{sat} - 1$.

The D_{PRI} parameter has greater impact on alteration at low flow rates or under static conditions because it controls the PRI formation phase with a duration of about $t_{PRI2} = D_{PRI}/r_{f2}^2$ as long as alteration is not yet controlled by precipitation. However, the value of this parameter is based on independent measurements, which allows to constrain its variation range.

Of all the model parameters, the precipitation law postulated in the analytical GRAAL model as $\frac{dM_{pr}}{dt} = \rho' k' S' \left(\frac{C_{Si}(t)}{C'_{sat}} - 1\right)$ (Eq. (3) and Section 2.2.3) not only has the greatest long-term impact, but is also difficult to fit with the available experimental data. Only an upper bound can be assigned to the kinetic parameter k' by comparison with tests under static or very low flow rate conditions: with reasonable confidence we can infer from the data that for SON68 glass altered at 90 °C in initially pure water, k' is less than 10^{-13} m s^{-1} (or more precisely, the product $k'(C_{sat}/C'_{sat} - 1)$ is less than 10^{-14} m s^{-1}). However, this constraint alone is insufficient to predict the quantity of altered glass over the long term, particularly since the simplified precipitation law (by comparison with the precipitation laws used in the geochemical GRAAL model) must still be validated and will also impact the sensitivity with respect to the C_{sat} parameter. The latter parameter has little impact as long as the precipitation kinetics are assumed to remain constant at saturation and the value of C'_{sat} is fitted accordingly.

In sum, the sensitivity study demonstrates that, provided the approximations made in the analytical GRAAL model and the expected discrepancies with the experimental observations, the parameter values proposed for the analytical GRAAL model (Table 2) are validated except for the precipitation law, for which experimental comparisons can only establish an upper limit on the kinetics at saturation, more precisely on the product $k'(C_{sat}/C'_{sat}-1)$. In other words the laboratory tests considered in this work cannot discriminate between a low precipitation rate combined to a low precipitation threshold (typical to the quartz) and a higher precipitation rate combined to a threshold nearer to the value of C_{sat}. Future work, based on modeling and specific tests, is necessary for assessing realistic values for both k' and C'_{sat}.

4. Application to a geological repository

The analytical GRAAL model is applied to a geological repository through a 1D Cartesian description of the package–barrier system that is justified not only for reasons of simplicity, but also by the convective–diffusive flow conditions prevailing in an actual repository. These conditions are illustrated in Fig. 10, in which U_{site} is the Darcy velocity for solute transport in the geological formations of the site, shown here, in this generic case, parallel to the package lengthwise direction. In this configuration the diffusion boundary layer depends in strict logic on the distance x from the bottom of the package, according to the relation $z(x)=\left(\frac{D_{barr}x}{U_{site}}\right)^{1/2}$.

In this application exercise, package alteration is described in a simplified manner by assuming the package is surrounded by a uniform and purely diffusive barrier of constant thickness L. Within this framework, the container and overpack corrosion product layer is not taken into account as a distinct medium. Moreover, the effect of geometry is disregarded, as it does not exceed the same order of magnitude as the effects of this simplification. Given the expected values for D_{barr} (effective diffusion coefficient in the barrier, about 10^{-11} m^2 s^{-1} [30]) and U_{site} (10^{-11} m s^{-1}, see [3], p. 468), the value of L does not exceed 1 m, corresponding to the thickness of the boundary layer at a distance from the bottom of the package equal to its height, H_{block} (1.1 m). The mean thickness to be taken into account is equal to $L_{eq}=\frac{2}{3}\left(\frac{D_{barr}H_{block}}{U_{site}}\right)^{1/2}$ or about 70 cm. This becomes the reference value for L, and a sensitivity study will be performed to take into account the differences in the thickness and the other package dimensions—especially its diameter $2R_{block}$ equal to 42 cm—which must be considered in the case of flow at an oblique or right angle to the package.

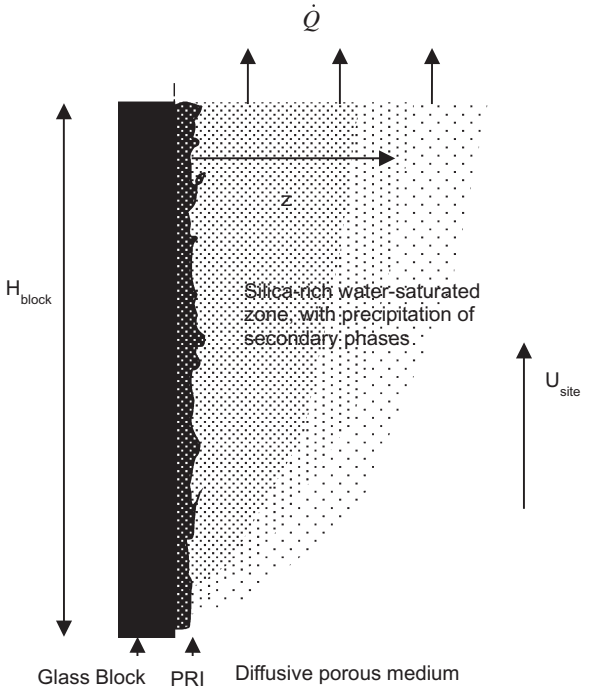

Fig. 10. Schematic representation of silica and boron plume around a glass package of height H subjected to alteration in an infinite permeable porous medium under convective–diffusive conditions in which the flow direction is parallel to the package. Note that z is the horizontal coordinate with respect to this figure, and x is the vertical coordinate.

For a package–barrier system described in 1D Cartesian coordinates with a barrier of finite thickness, the system of equations is comparable to Eqs. (1)–(5) for a homogeneous medium, except that the barrier is described as a diffusive and reactive medium and the precipitation of neoformed phases is taken into account both at the glass/barrier interface and within the barrier. This gives a total of eight equations, detailed in Appendix B:

- Five equations concerning silicon:
  (1) an equation describing the PRI dissolution kinetics,
  (2) an equation describing the precipitation kinetics of neoformed phases at the glass–barrier interface,
  (3) an equation describing the precipitation kinetics of neoformed phases in the barrier,
  (4) an equation for the silicon mass balance at the glass–barrier interface, and
  (5) an equation for silicon transport in the barrier.
- Three equations concerning boron:
  (6) an equation describing the PRI formation kinetics,
  (7) an equation for the boron mass balance at the glass–barrier interface, and
  (8) an equation for boron transport in the barrier.

The boundary conditions are assumed to be constant silicon and zero boron concentrations outside the barrier, and the initial condition is a constant silicon and zero boron concentration in the barrier.

The equations are solved with a focus on silicon because the primary objective of the analytical GRAAL model applied to a repository is to predict quantity of altered glass and the overall alteration rate. For this purpose, only the Eqs. (1)–(6) are to be considered..

The parameters used in the analytical GRAAL model applied to a repository are those of the model itself, which have already been described in Part 2. The additional parameters describing the package and the repository are indicated below (Section 4.1.1).

4.1. GRAAL equations and solutions in the case of a diffusive barrier with precipitation in the barrier and no constant final rate (1D Cartesian)

4.1.1. Nomenclature

Description of the glass block:

- H_{block}, m: height of the glass block
- R_{block}, m: radius of the glass block
- $\Omega_{block}=\pi R^2_{block}H_{block}$, m^3: volume of the glass block
- $M_{block}=\rho_{glass}\Omega_{block}$, kg: mass of the glass block
- $S_{mono}=2\pi R_{block}(H_{block}+R_{block})$, m^2: monolithic surface of the glass block
- τ_F: fracture ratio of the glass block
- $S=\tau_F S_{mono}$, m^2: reactive surface area of the glass block, taking into account fracturing

Description of the barrier system:

- z, m: distance inside the barrier
- $C_{Si}(z,t)$, mol m^{-3}: silicon concentration profile in the barrier at time t
- $C_B(z,t)$, mol m^{-3}: boron concentration profile in the barrier at time t
- $m_{pr}(z,t)$, kg m^{-3}: profile of precipitate in the barrier at time t
- $z_{pr}(t)$, m: position of the precipitation front at time t after the onset of precipitation (t_{opr})
- $l(t) = \left(\frac{\pi D_{barr} t}{\omega}\right)^{1/2}$, m: position of the diffusion front in the barrier at time t (linearized silicon profile)
- $C_{Si\_opr}(z)$: silicon concentration profile in the barrier at the onset of precipitation (t_{opr})
- σ', m^{-1}: surface of precipitation in the barrier per unit volume
- ω: porosity of the barrier
- D_{barr}, m^2 s^{-1}: effective diffusion coefficient of Si in the barrier
- U_{site}, m s^{-1}: Darcy velocity for solute transport in the geological formations of the site
- L, m: thickness of the barrier. A reasonable value of L can be estimated by taking into account the diffusion in the barrier and convection around the barrier
- Ω, m^3: free volume of water between the glass block and the barrier ($\Omega \to 0$)
- Σ, m^2: section of the barrier ahead of the glass block

4.1.2. Equations

The equations for PRI dissolution and formation, for silicon and boron material balance at the glass/barrier interface, and for silicon and boron transport in the barrier are given in Appendix B. The equations for the precipitation of neoformed phases are the following:

- Precipitation at the glass/barrier interface:

$$\frac{\partial M_{pr}(0,t)}{\partial t} = \rho' k' S' \left(\frac{C_{Si}(0,t)}{C'_{sat}} - 1\right)$$
$$\text{if } M_{pr}(0,t) > 0 \quad \text{or} \quad C_{Si}(0,t) > C'_{sat};\ 0 \text{ otherwise} \qquad (14)$$

- Precipitation in the barrier:

$$\frac{\partial m_{pr}(z,t)}{\partial t} = \rho' k' \sigma' \left(\frac{C_{Si}(z,t)}{C'_{sat}} - 1\right)$$
$$\text{if } m_{pr}(z,t) > 0 \quad \text{or} \quad C_{Si}(z,t) > C'_{sat};\ 0 \text{ otherwise} \qquad (15)$$

In other words, the same precipitation threshold, C'_{sat}, is used at the glass/barrier interface and in the barrier.

4.1.3. Input parameter values for application to a repository

The reference values for the additional parameters concerning the geological repository are indicated in Table 6. The other parameters are the same as for a homogeneous medium, and are indicated in Table 2 (Section 2.3).

- The package geometric parameters are the same for any R7T7-type package, and the fracture ratio is the value adopted for the models used to date ($V_0 \to V_r$ model [31]).
- The barrier transport parameters (D_{barr}, ω) are determined from measurements in clay. The barrier thickness was estimated for a flow velocity U_{site} of 10^{-11} m s^{-1}, corresponding to the range of the Darcy velocity values for solute transport in the French disposal site at Bure (10^2–10^3 m Myr^{-1}, see [3], p. 468).
- As in the comparison with laboratory tests, the precipitate surface area at the glass/barrier interface is assumed equal to the total package surface area (68 m^2) which implies that precipitation occurs in the immediate vicinity of the reaction interface.

Table 6
Additional parameter values of analytical GRAAL model applied to a geological repository (reference values).

Parameter	Notation/unit	Value
Package radius	R_{block} (m)	0.21
Package height	H_{block} (m)	1.1
Package volume	Ω_{block} (m^3)	0.15
Monolithic package surface area	S_{mono} (m^2)	1.7
Package fracture ratio	τ_F	40
Glass block surface area taking fracturing into account	S (m^2)	68
Barrier thickness	L (m)	0.7
Barrier porosity	ω	0.2
Effective Si diffusion coefficient in the barrier	D_{barr} (m^2 s^{-1})	10^{-11}
Barrier cross section facing glass block	Σ (m^2)	1.7
Free volume of water between glass block and barrier	Ω (m^3)	0
Ratio of precipitation surface area at the glass/barrier interface to glass surface area	S'/S	1
Precipitation surface area per unit volume in the barrier	σ' (m^{-1})	10^6

- Precipitation in the barrier is dealt with by assuming a precipitate surface area per unit volume σ of 10^6 m^{-1}; this is a realistic value for compact clays such as FoCa7 bentonite [32]; for this value, the precipitation of a significant mass occurs within the barrier compared with precipitation at the package/barrier interface. The proposed value is lower than that would be obtained by taking into account the maximum possible area (the developed pore surface area [32]), i.e. a value of 4×10^7 m^{-1}. Note that lower values of σ', around 10^4 m^{-1}, have been used as a base for chemistry–transport studies in the barrier [33].
- The value of the constant silicon concentration in the barrier taken as an initial value and a boundary condition is set to zero, as a simplification in this modeling exercise. This assumption remains realistic with respect to the French repository site since the in-situ measurements provide silicon concentrations around 0.14 mol m^{-3} [34], compatible with a model solution reference value of 0.18 mol m^{-3} at 25 °C [35]. Even when extrapolating the model solution to 90 °C, the silicon concentration would not exceed 0.85 mol m^{-3}. This is much lower than both the saturation value (C_{sat} = 2.0 mol m^{-3}) and the precipitation threshold (C'_{sat} = 1.9 mol m^{-3}) considered in this study.

4.1.4. Solution of equations – main characteristic quantities

The detailed solution of the equations is described in Appendix B for the PRI formation and dissolution rate, the silicon profile in the barrier, and the altered thickness. Alteration occurs in three phases:

- An initial phase during which the alteration rate diminishes without any precipitation, as long as the silicon concentration at the glass/barrier interface remains below C'_{sat}. This phase is very brief.
- The onset of precipitation (t_{opr}) marks the beginning of a phase during which the alteration rate diminishes with precipitation at the glass/barrier interface and in the barrier (the model assumes a single precipitation threshold equal to C'_{sat}). During this phase, the zero concentration boundary condition outside the barrier implies the existence of a precipitation front, $z_{pr}(t)$, progressing within the barrier.
- After a time equivalent to the diffusion time through the barrier (t_{pbarr}), a steady-state profile is established and steady-state alteration conditions are reached with a final rate, r_f.

Theoretically, the system of equations concerning silicon can be solved analytically before the onset of precipitation ($t < t_{opr}$),

whereas once this threshold is exceeded a numerical solution is required to take into account the precipitation front in the barrier. However, an approximate analytical solution is possible if a quasi-steady state diffusion profile is assumed in the barrier with a thickness equal to the diffusion length: $l(t) = \left(\frac{\pi D_{barr} t}{\omega}\right)^{1/2}$. The silicon concentration is therefore assumed equal to zero for $z = l(t)$. A steady-state diffusion profile then exists in the barrier; it is nonlinear between 0 and $z_{pr}(t)$ (precipitation front), and linear between $z_{pr}(t)$ and $l(t)$. By taking into account the flow boundary conditions at the precipitation front and at the glass/barrier interface it is then possible to determine the diffusion profile, the progress of the precipitation front $z_{pr}(t)$, and to compute the PRI dissolution rate. This approximation of steady-state conditions can be justified by comparing the approximated and exact approaches to the PRI dissolution rate before the onset of precipitation (see Appendix B, Section B.3.3).

The main characteristic quantities concerning package alteration in a geological repository are indicated in Table 7.

The analytical expressions of the alteration rates and altered thicknesses are given in Appendix B, Section B.4. It can be shown that in most cases, the PRI dissolution rate decreases in $t^{1/2}$ from the time t_{ibarr2} (characteristic time of inflexion for the alteration rate due to silicon diffusion in the barrier), until the final alteration rate (r_f) is reached.

Table 7
Characteristic times and quantities for the analytical GRAAL model applied to the alteration of a glass package in a geological repository with a diffusion barrier.

Characteristic time/quantity	Definition
$t_{pbarr} = \frac{\omega L^2}{\pi D_{barr}}$	Diffusion time through the barrier
$t_{ibarr1} = \frac{\omega D_{barr}}{\pi r_{disso}^2}\left(\frac{\Sigma C_{sat}}{S C_{vSi}}\right)^2 = \frac{\omega \delta_1^2}{\pi D_{barr}}$	Characteristic time of inflexion of glass alteration rate, due to silicon diffusion in the barrier, in the absence of precipitation
$t_{ibarr2} = \frac{\omega D_{barr}}{\pi}\left(\frac{\Sigma C_{sat}}{S C_{vSi} r_{disso} + \rho' k' S' \frac{C_{sat}}{C'_{sat}}}\right)^2$	Characteristic time of inflexion of glass alteration rate, due to the silicon diffusion in the barrier, taking into account the precipitation at the glass/barrier interface
$t_{opr} = \frac{t_{ibarr1}}{\left(\frac{C_{sat}}{C'_{sat}} - 1\right)^2}$	Time to onset of precipitation
$\delta_1 = \frac{\Sigma D_{barr} C_{sat}}{S C_{vSi} r_{disso}}$	Characteristic length of diffusion of the silicon in the barrier, in the absence of precipitation
$\delta_2 = \frac{\Sigma D_{barr} C_{sat}}{S C_{vSi} r_{disso} + \rho' k' S' \frac{C_{sat}}{C'_{sat}}}$	Characteristic length of diffusion of the silicon in the barrier, taking into account the precipitation at the glass/barrier interface
$\delta'_0 = \left(\frac{C_{sat} D_{barr}}{\rho' k' \sigma'}\right)^{1/2}$	Characteristic length of the precipitation layer in the barrier under steady-state conditions
$p' = \left(\frac{\rho' k' \sigma'}{C_{sat} D_{barr}}\right)^{1/2} \frac{\Sigma D_{barr} C_{sat}}{S C_{vSi} r_{disso} + \rho' k' S' \frac{C_{sat}}{C'_{sat}}}$	Ratio δ_2/δ'_0 of characteristic lengths of diffusion to precipitation in the barrier, indicative of the importance of the precipitation phenomenon
$r_f = r_{disso}\left(1 - \frac{C'_{sat}}{C_{sat}} \frac{1 + F - \Delta^{1/2} - p'^2}{1 - p'^2}\right)$	Final rate, taking account diffusion and precipitation in the barrier and around the glass block, for a finite barrier
where $\Delta = (Fp')^2 + \frac{\delta_2^2}{L^2}(1 - p'^2)$	
$F = \frac{\delta_2}{\delta_1}\left(\frac{C_{sat}}{C'_{sat}} - 1\right) = \frac{S C_{vSi} r_{disso}\left(\frac{C_{sat}}{C'_{sat}} - 1\right)}{S C_{vSi} r_{disso} + \rho' k' S' \frac{C_{sat}}{C'_{sat}}}$	
$r_{f0} = r_{disso}\left(1 - \frac{C'_{sat}}{C_{sat}} \frac{1 + F + p'}{1 + p'}\right) = r_{disso}\left(1 - \frac{C'_{sat}}{C_{sat}}\right)\Theta$	Final rate, taking account diffusion and precipitation in the barrier and around the glass block, for an infinite barrier
$\Theta = \frac{\rho' k' S' \frac{C_{sat}}{C'_{sat}} + (\rho' k' \sigma' D_{barr} C_{sat})^{1/2} \Sigma}{S C_{vSi} r_{disso} + \rho' k' S' \frac{C_{sat}}{C'_{sat}} + (\rho' k' \sigma' D_{barr} C_{sat})^{1/2} \Sigma}$	
$t_{PRI} = \frac{D_{PRI}}{r_f^2}; \lambda_{PRI} = \frac{D_{PRI}}{r_f}$	Characteristic time of formation, characteristic thickness of the PRI

4.2. Results

4.2.1. Calculations with reference values at 90 °C

The additional parameter values relative to the geological repository are indicated in Table 6 (Section 4.1.3). The other parameters are the same as for a homogeneous medium, and are indicated in Table 2 (Section 2.3).

With these reference parameter values, the principal characteristic quantities are indicated in Table 8. The evolution of the altered glass thickness ($E(t) + e(t)$), the PRI thickness ($e(t)$) and the glass alteration rate ($r(t)$) are indicated in Fig. 11.

Table 8
Values of main characteristic quantities obtained with the reference parameters.

Diffusion time through the barrier	t_{pbarr} (yrs)	9.9×10^{1}
Time of inflexion without precipitation	t_{ibarr1} (yrs)	4.1×10^{-8}
Time to onset of precipitation	t_{opr} (yrs)	1.5×10^{-5}
Time of inflexion with precipitation at the glass/barrier interface	t_{ibarr2} (yrs)	4.0×10^{-8}
Diffusion length in the barrier with precipitation at glass/barrier interface	δ_2 (m)	1.4×10^{-5}
Precipitation length in the barrier	δ'_0 (m)	2.2×10^{-4}
Precipitation/diffusion length ratio in the barrier	p'	6.3×10^{-2}
Final rate (finite barrier)	r_f (m s^{-1})	6.0×10^{-15}
Final rate with an infinite barrier	r_{f0} (m s^{-1})	6.0×10^{-15}
Characteristic time of PRI formation	t_{PRI} (yrs)	2.7×10^{-1}
Maximum PRI thickness	λ_{PRI} (m)	5.0×10^{-8}

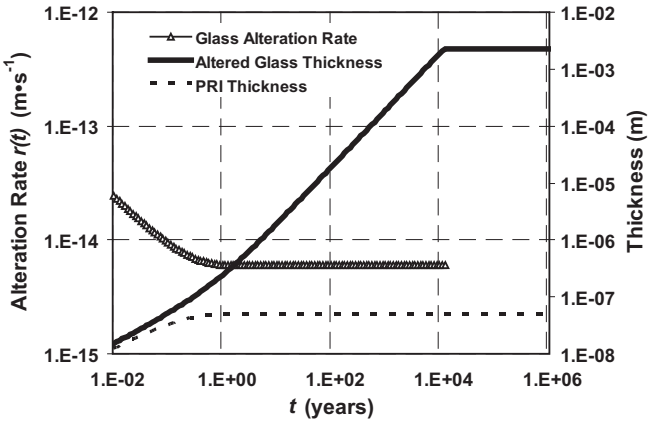

Fig. 11. Altered glass thickness ($E(t) + e(t)$), PRI thickness ($e(t)$), and glass alteration rate ($r(t)$, m s^{-1}) versus time for a glass block altered in the presence of a diffusion barrier, with the reference parameters. Alteration of the whole package is equivalent to a total altered thickness of 2.2 mm (ratio of the block volume to the initial glass surface area accessible to water, taking into account a fracture ratio of 40).

With the reference values, the onset of precipitation (t_{opr}) is reached very quickly (about 10 min); the phase before C'_{sat} is reached at the reaction interface is therefore always of very short duration. The diffusion time through the barrier (t_{pbarr}) is reached after about 100 years; this is due to the effect of the useful barrier thickness, limited to 70 cm, beyond which convection imposes "zero silicon concentration" boundary conditions. However, it can be seen that the final alteration regime is reached within less than a year, much shorter than the diffusion time through the barrier. This indicates that under these conditions precipitation is the driving mechanism of glass alteration, much more than silicon diffusion through the barrier.

The PRI effect predominates for up to a few months, and concerns an altered glass fraction of about 0.01% of the block mass. Silicon dissolution thereafter predominates in the package alteration process, and decreases at a rate roughly equal to $t^{1/2}$ until a final rate of about 6×10^{-15} m s^{-1} (i.e. 3×10^{-3} r_{disso}) is reached after about 1 year.

Beyond 1 year the system is under residual rate conditions controlled by the precipitation kinetics of the silicated phase. This stage proceeds until alteration of the whole package, equivalent to a thickness of 2.2 mm, is reached after 11,000 years at 90 °C, when the precipitation in the barrier is taken into account.

4.2.2. Sensitivity calculations

The sensitivity study concerns:

- the model physical parameters: hydration rate r_{hydr}, initial PRI dissolution rate r_{disso}, precipitation rate k', diffusion coefficient in the PRI D_{PRI}, silicon concentration at saturation C_{sat}, and
- the repository parameters: precipitate surface area in the barrier σ' (precipitate surface area per unit barrier volume) and the barrier thickness L.

The parameters examined are listed in Table 9.

The comparison is done for each parameter in the following discussion and illustrated in Figs. 12–15). It concerns the glass alteration rate $r(t)$, the altered glass thickness ($E(t) + e(t)$) and the PRI thickness ($e(t)$).

Unsurprisingly, the comparison demonstrates that the parameters describing the initial alteration kinetics (r_{hydr} and r_{disso}), have very little influence outside the initial instants of alteration (a few seconds to a few minutes) except, in the case of r_{disso}, if the precipitation surface area in the barrier is very high, in which case the final alteration rate approaches $r_{disso}(1 - C'_{sat}/C_{sat})$ and thus depends on the value of this parameter.

The effect of the diffusion coefficient in the PRI (D_{PRI}) is proportional to the PRI thickness. It has a significant effect as long as the PRI thickness is an appreciable fraction of the total altered glass thickness, i.e. for about a year and for altered thicknesses up to about a hundred nanometers, corresponding to altered glass fraction of up to 0.01% (in this study, package core alteration corresponds to an altered glass thickness of 2.2 mm because of fracturing). Beyond these thicknesses, the impact of the PRI is negligible.

The silicon concentration at saturation (C_{sat}) has little effect on the initial and intermediate alteration regimes, but affects the final alteration rate. This effect is significant if C_{sat} varies while maintaining a constant precipitation threshold value C'_{sat} (Table 10 and Fig. 12), but is much smaller if C'_{sat} is fitted proportionally to C_{sat}.

The magnitude of this effect is expected because the final alteration rate, given here for an infinite barrier (see Table 7) by the expression:

$$r_{f0} = r_{disso}\left(1 - \frac{C'_{sat}}{C_{sat}}\right)\frac{\rho' k' S' \frac{C_{sat}}{C'_{sat}} + \left(\rho' k' \sigma' D_{barr} C_{sat}\right)^{1/2}\Sigma}{SC_{vSi} r_{disso} + \rho' k' S' \frac{C_{sat}}{C'_{sat}} + \left(\rho' k' \sigma' D_{barr} C_{sat}\right)^{1/2}\Sigma} \tag{16}$$

depends mainly on the value of $C_{sat}/C'_{sat} - 1$, or $1 - C'_{sat}/C_{sat}$ according to the extent of precipitation in the barrier. As in the reference case $C_{sat}/C'_{sat} - 1 = 1/19$, the final rate can increase significantly as soon as C_{sat} deviates from the reference value of C'_{sat}, 1.9 mol m^{-3}. On the other hand, if C'_{sat}/C_{sat} is constant, the final rate is at most proportional to $C_{sat}^{1/2}$ should the precipitation term in the barrier be predominant, and independent from C_{sat} in the other cases.

The precipitation kinetics parameter (k', Fig. 13) as expected, has a negligible effect on the initial and intermediate alteration regimes, and a major effect on the final alteration rate, also illustrated by the expression for r_{f0} in Eq. (16). Depending on the extent of precipitation in the barrier, its effect will be proportional to the value of k' or to the square root of this parameter. Given the reference values, the second case is applicable here: the final rate varies by a factor of 5 (from 2.9×10^{-15} to 1.4×10^{-14} m s^{-1} for a k' value varying by a factor of 20 (from 5×10^{-15} to 1×10^{-13} m s^{-1}).

The effect of precipitation in the barrier, which is tested by varying the precipitation surface area per unit volume σ' (Fig. 14), also has a significant influence on the final alteration regime and is negligible for the initial and intermediate regimes. When this effect is significant with respect to precipitation at the glass/barrier interface, the final rate rises above the minimum value of 1.0×10^{-15} m s^{-1} obtained by assuming precipitation occurs at the glass/barrier interface alone, then increases proportionally to the square root of σ' to the maximum value of $r_{disso}(1 - C'_{sat}/C_{sat})$ equal to 8.5×10^{-14} m s^{-1}. Given the reference values, the final rate increases from 1.2×10^{-15} to 3.3×10^{-14} m s^{-1} when σ' ranges from 10^3 to 10^8 m^{-1}.

The effect of the barrier thickness (L, Fig. 15), becomes appreciable only after the diffusion time through the barrier t_{pbarr}, although only barriers less than about 1 cm thick induce a significant effect. This is due to the effect of precipitation, which imposes a final alteration rate higher than the rate induced by the diffusive flow through the barrier except for very small thicknesses: with a 3 mm barrier the final rate is only twice that if an infinite diffusion barrier. In fact it is possible to estimate the barrier thickness L for which the diffusive flow is of the same order of magnitude as the flow arising from the precipitation sink term:

$$L_{crit} = \frac{\Sigma}{S}\frac{D_{barr}}{r_{f0}}\frac{C_{sat}}{C_{vSi}} \tag{17}$$

Table 9
Reference, minimum (or intermediate) and maximum parameter values of GRAAL model applied to glass package alteration in a repository at 90 °C.

Parameter	Notation/unit	Reference value	Minimum or intermediate value	Maximum value
PRI dissolution rate	r_{disso} (m s^{-1})	1.7×10^{-12}	1.0×10^{-12}	9.0×10^{-12}
Rate of pristine glass hydration forming the PRI	r_{hydr} (m s^{-1})	10^{-11}	3×10^{-12}	10^{-7}
Diffusion coefficient in the PRI	D_{PRI} (m^2 s^{-1})	3×10^{-22}	6×10^{-23}	6×10^{-22}
Total Si concentration at saturation ($C'_{sat} = 0.95C^{sat}$)	C_{sat} (mol m^{-3})	2.0	1.0	4.0
Total Si concentration at saturation (C'_{sat} constant at 1.9 mol m^{-3})	C_{sat} (mol m^{-3})	2.0	3.0	4.0
Kinetic parameter for neoformed phase precipitation	k' (m s^{-1})	2×10^{-14}	5×10^{-15}	1×10^{-13}
Precipitation surface area per unit volume in the barrier	σ' (m^{-1})	10^6	10^3	10^8
Barrier thickness	L (m)	0.7	0.003	1.0

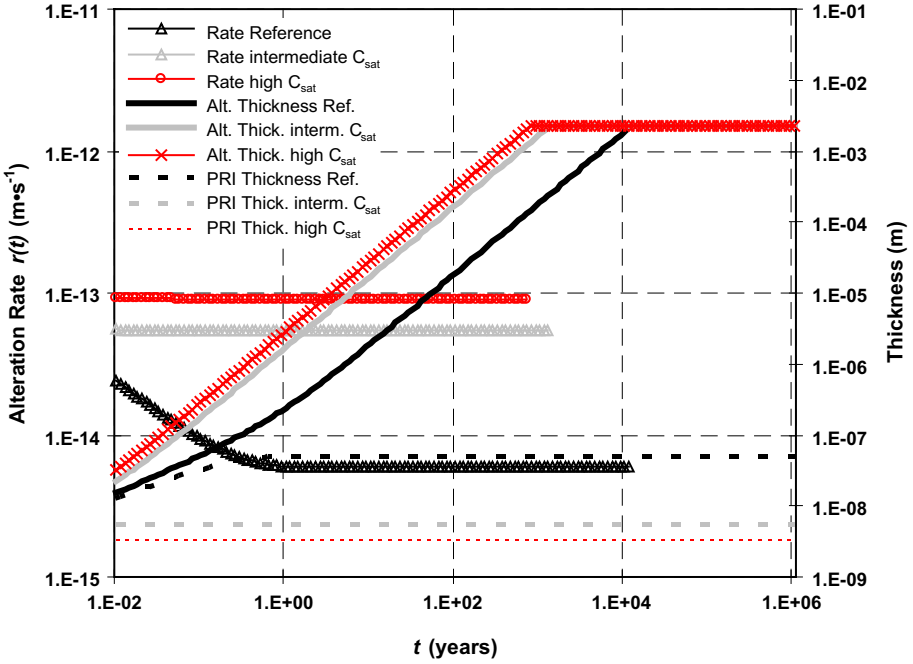

Fig. 12. Altered glass thickness, PRI thickness, and glass alteration rate ($r(t)$, m s^{-1}) versus time for a glass block altered in the presence of a barrier, for different silicon concentrations at saturation (C_{sat}), assuming a precipitation threshold C'_{sat} equal to 1.9 mol m^{-3}. The reference, intermediate and high value for C_{sat} are respectively 2.0, 3.0 and 4.0 mol m^{-3}.

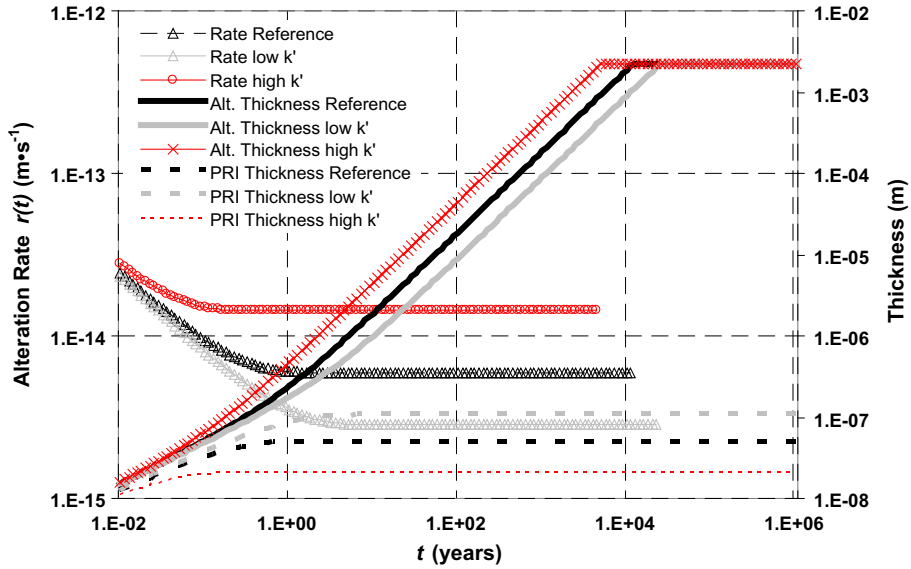

Fig. 13. Altered glass thickness, PRI thickness, and glass alteration rate ($r(t)$, m s^{-1}) versus time for a glass block altered in the presence of a barrier, for different secondary silica phase precipitation rate parameter values (k'). The reference, low and high value for k' are respectively 2×10^{-14}, 5×10^{-15} and 1×10^{-13} m s^{-1}.

For the reference values of the analytical GRAAL model at 90 °C, the critical thickness is 4 mm; at the minimum residual rate obtained by disregarding precipitation in the barrier ($r_{f0} = 1.0 \times 10^{-15}$ m s^{-1}), L_{crit} becomes 2.5 cm, a value much lower than the effective thicknesses under convective–diffusive conditions (several tens of centimeters). However, because the residual rate r_{f0} is expected to be much more temperature-dependent than D_{barr} and C_{sat}, it is possible that at temperatures more representative of a repository (30–50 °C) the critical thickness L_{crit} becomes comparable to or even exceeds the effective barrier thickness. This issue is discussed in Section 4.2.4 with regard to low temperature applications.

4.2.3. Discussion and summary concerning application of the model to a repository at 90 °C

For the application of the analytical GRAAL model to glass package alteration in the presence of a diffusion barrier at 90 °C, not only the calculations with the model reference values (Section 4.2.1) but also the sensitivity study (Section 4.2.2) indicate that:

1. Most of the package alteration takes place under final rate conditions, which are reached after a few years with a total altered glass fraction of less than 0.1%.
2. The final rate regime is controlled by secondary phase precipitation both at the glass/barrier interface and in the barrier. A

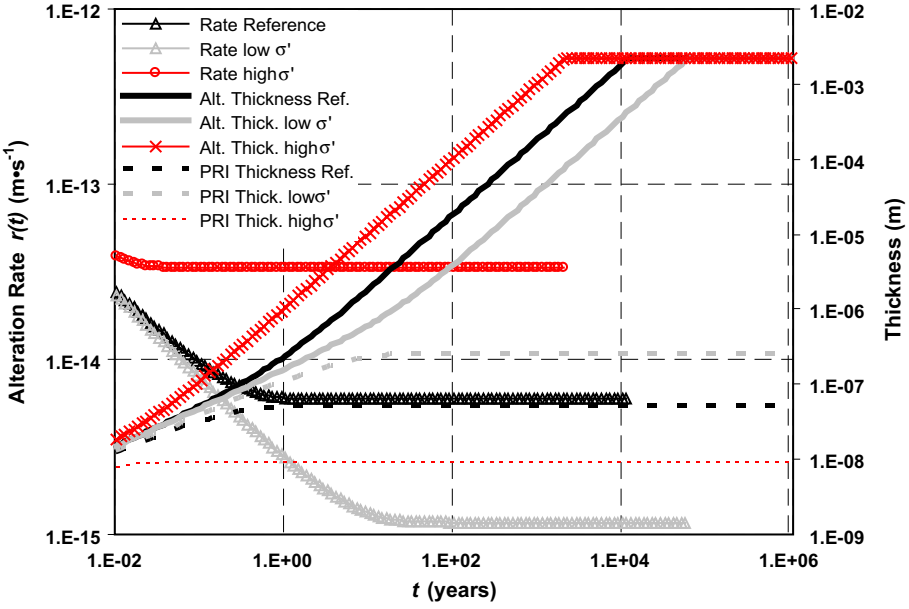

Fig. 14. Altered glass thickness, PRI thickness, and glass alteration rate ($r(t)$, m s^{-1}) versus time for a glass block altered in the presence of a barrier, for different precipitation surface areas per unit volume in the barrier (σ'). The reference, low and high value for σ' are respectively 10^6, 10^3 and 10^8 m^{-1}.

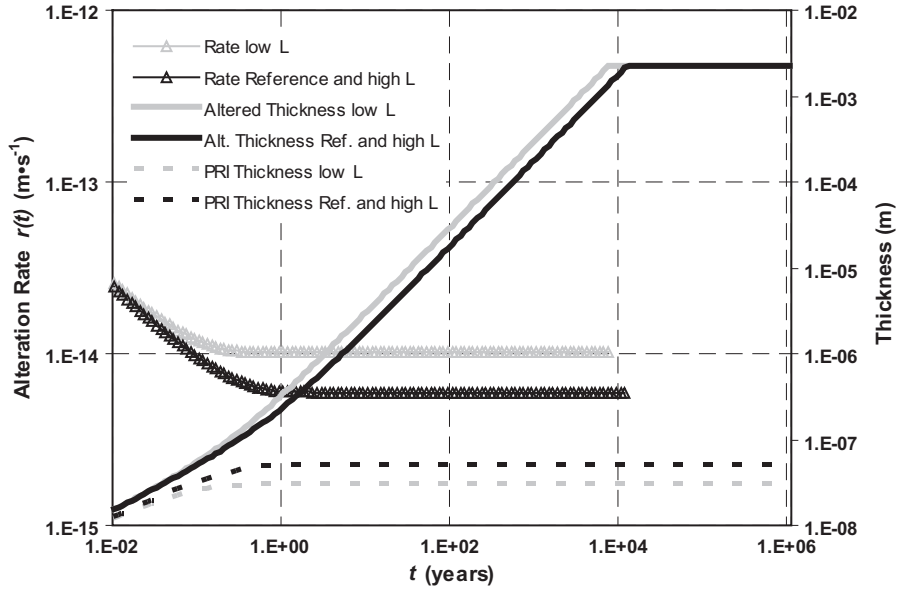

Fig. 15. Altered glass thickness, PRI thickness, and glass alteration rate ($r(t)$, m s^{-1}) versus time for a glass block altered in the presence of a barrier, for different barrier thicknesses L = 0.7 m (reference), 0.003 m (low) and 1.0 m (high). The results for L = 0.7 and 1.0 m are nearly identical.

simplified expression of this final rate is proposed, assuming an infinite barrier, by the relation:

$$r_{f0} = r_{\text{disso}}\left(1 - \frac{C'_{sat}}{C_{\text{sat}}}\right)\frac{\rho' k' S' \frac{C_{\text{sat}}}{C'_{\text{sat}}} + \left(\rho' k' \sigma' D_{\text{barr}} C_{\text{sat}}\right)^{1/2}\Sigma}{SC_{\text{vSi}} r_{\text{disso}} + \rho' k' S' \frac{C_{\text{sat}}}{C'_{\text{sat}}} + \left(\rho' k' \sigma' D_{\text{barr}} C_{\text{sat}}\right)^{1/2}\Sigma} \quad (18)$$

In the reference case, the final rate is equal to r_{f0}, or 6.0×10^{-15} m s^{-1}. This corresponds to alteration of the whole package (an altered thickness of 2.2 mm) after 11,000 years at 90 °C.

3. The parameters describing the initial stages of alteration (r_{hydr} and r_{disso}) have very little influence on alteration after a very short time—a few minutes—unless precipitation in the barrier is massive enough to impose a concentration at the reaction interface near C'_{sat} and thus an alteration rate near $r_{\text{disso}}(1 - C'_{\text{sat}}/C_{\text{sat}})$
4. The PRI has a significant effect during the initial and intermediate stages of alteration, but is limited by the PRI thickness at the final rate $\lambda_{PRI0} = D_{\text{PRI}}/r_{f0}$. Assuming the minimum value for r_{f0} (10^{-15} m s^{-1}) and the maximum value for D_{PRI} (6×10^{-22} m^2 s^{-1}), it would be 600 nm thick, equivalent to an altered glass fraction of less than 0.03%.
5. The effect of the barrier thickness is negligible because the alteration rate due to precipitation is faster than the rate due to diffusive flow through the barrier unless it is very thin (less than 1 cm).
6. The parameters related to precipitation (precipitation kinetics k', precipitation surface area in the barrier σ', precipitation threshold C'_{sat}) as well as the concentration at saturation C_{sat}, have a significant effect on package alteration that can be quantified by their impact on the final rate r_{f0} in relation

Table 10
Final alteration rate (r_f) versus silicon concentration at saturation (C_{sat}) and precipitation threshold (C'_{sat}).

C_{sat} (mol m^{-3})	C'_{sat} (mol m^{-3})	r_f (m s^{-1})
1.0	0.95	4.6×10^{-15}
2.0 (ref)	**1.9 (ref)**	**6.0×10^{-15}**
4.0	3.8	7.9×10^{-15}
3.0	1.9	5.5×10^{-14}
4.0	1.9	9.1×10^{-14}

(18). In particular, if precipitation in the barrier has little impact the package lifetime increases from 11,000 to 60,000 years at 90 °C.

As a result of this study, it may be assumed as a first approximation that the package is altered at r_{f0}, after a brief initial phase dominated by a rate drop as a function of $t^{1/2}$ during which the PRI dissolution rate is near $r_{Si}(t) \approx r_{disso}(t_{ibarr2}/t)^{1/2}$, and at the same time by the creation of a PRI with a maximum thickness of $\lambda_{PRI0} = D_{PRI}/r_{f0}$. These are the essential results obtained by applying the simplified GRAAL model, and are summarized in Tables 11–13 according to the model parameter values. They include:

- The characteristic time of PRI formation:

$$t_{PRI} = \frac{D_{PRI}}{r_{f0}^2} \tag{19}$$

- The equivalent altered glass fraction corresponding to the maximum PRI thickness:

$$AGF_{PRImax} = \frac{D_{PRI}}{r_{f0}} \frac{S}{\Omega_{block}} \tag{20}$$

- The time to reach a steady-state silicon concentration

$$t_{Si\_stat} \approx t_{ibarr1} \left(\frac{r_{disso}}{r_{f0}}\right)^2 = \frac{\omega D_{barr}}{\pi r_{f0}^2} \left(\frac{\Sigma C_{sat}}{S C_{vSi}}\right)^2 \tag{21}$$

- The altered glass fraction equivalent to the PRI thickness dissolved during the transient phase

$$AGF_{Si\_stat} = 2 r_{f0} t_{Si\_stat} = \frac{2\omega D_{barr}}{\pi r_{f0}} \left(\frac{\Sigma C_{sat}}{S C_{vSi}}\right)^2 \tag{22}$$

- The total package lifetime

$$t_{total\_block} \approx \frac{\Omega_{block}}{S r_{f0}} \tag{23}$$

The results reported in Tables 11 and 12 confirm that the transient phases are of short duration, generally a few days for the silicon transient (PRI dissolution) and a few months a or few years for the formation of the PRI (the time is inversely proportional to the final alteration corresponding to precipitation in the barrier). The corresponding altered glass fractions are about 10^{-4}% for the inherent silicon transient and 10^{-3}% to 10^{-2}% for the PRI thickness.

The package lifetime indicated in Table 13, slightly exceeds 10,000 years with this set of parameter values, especially the precipitation surface area in the barrier, σ', assumed equal to 10^6 m^{-1}. With a smaller value (10^3 m^{-1}), the package lifetime increases to 60,000 years at 90 °C. The choice of the precipitation kinetics parameter, k', is also decisive, as is the C_{sat} value, particularly when it diverges from C'_{sat} (1.9 mol m^{-3}). These results clearly illustrate that the choice of a precipitation law and the value assigned to C_{sat} are decisive for package alteration in a geological barrier, as well as for the effects of the container and overpack metallic corrosion products (CP) surrounding the package, for which it may be necessary to assess specifically the precipitation parameters (σ'_{CP} as well as k'_{CP}).

Table 13
Simplified calculation of the impact of GRAAL model parameters on the total package lifetime at 90 °C.

	Parameter value		Glass block lifetime (years)	
	Min	Max	Param. Min	Param. Max
r_{disso} (m s^{-1})	1.0×10^{-12}	9.0×10^{-12}	1.2×10^4	1.1×10^4
D_{PRI} (m^2 s^{-1})	6.0×10^{-23}	6.0×10^{-22}	1.1×10^4	1.1×10^4
C_{sat} (mol m^{-3})	1.0	4.0	1.5×10^4	8.7×10^3
C_{sat} (C'_{sat} = const)	2.0	4.0	1.1×10^4	7.5×10^2
k' (m s^{-1})	5.0×10^{-15}	1.0×10^{-13}	2.4×10^4	4.8×10^3
σ' (m^{-1})	1.0×10^3	1.0×10^8	5.8×10^4	2.0×10^3

Table 11
Simplified calculation of the impact of GRAAL model parameters on the PRI formation time and maximum altered glass fraction due to the formation of the PRI.

	Parameter value		t_{PRI} (years)		AGF_{PRImax}	
	Min	Max	Param. Min	Param. Max	Param. Min	Param. Max
r_{disso} (m s^{-1})	1.0×10^{-12}	9.0×10^{-12}	2.9×10^{-1}	2.4×10^{-1}	2.5×10^{-5}	2.2×10^{-5}
D_{PRI} (m^2 s^{-1})	6.0×10^{-23}	6.0×10^{-22}	5.4×10^{-2}	5.4×10^{-1}	4.7×10^{-6}	4.7×10^{-5}
C_{sat} (mol m^{-3})	1.0	4.0	4.6×10^{-1}	1.5×10^{-1}	3.1×10^{-5}	1.8×10^{-5}
C_{sat} (C'_{sat} = const)	2.0	4.0	2.7×10^{-1}	1.2×10^{-3}	2.3×10^{-5}	1.5×10^{-6}
k' (m s^{-1})	5.0×10^{-15}	1.0×10^{-13}	1.2	4.7×10^{-2}	4.9×10^{-5}	9.8×10^{-6}
σ' (m^{-1})	1.0×10^3	1.0×10^8	6.9	8.5×10^{-3}	1.2×10^{-4}	4.2×10^{-6}

Table 12
Simplified calculation of the impact of GRAAL model parameters on the steady-state silicon concentration onset time and the altered glass fraction equivalent to the PRI thickness dissolved during the transient phase.

	Parameter value		t_{Si_stat}(years)		AGF_{Si_stat}	
	Min	Max	Param. Min	Param. Max	Param. Min	Param. Max
r_{disso} (m s^{-1})	1.0×10^{-12}	9.0×10^{-12}	3.6×10^{-3}	2.9×10^{-3}	6.1×10^{-7}	5.5×10^{-7}
D_{PRI} (m^2 s^{-1})	6.0×10^{-23}	6.0×10^{-22}	3.3×10^{-3}	3.3×10^{-3}	5.8×10^{-7}	5.8×10^{-7}
C_{sat} (mol m^{-3})	1.0	4.0	1.4×10^{-3}	7.6×10^{-3}	1.9×10^{-7}	1.8×10^{-6}
C_{sat} (C'_{sat} = const)	2.0	4.0	3.3×10^{-3}	7.6×10^{-3}	5.8×10^{-7}	1.5×10^{-7}
k' (m s^{-1})	5.0×10^{-15}	1.0×10^{-13}	1.5×10^{-2}	5.8×10^{-4}	1.2×10^{-6}	2.4×10^{-7}
σ' (m^{-1})	1.0×10^3	1.0×10^8	8.6×10^{-2}	1.1×10^{-4}	3.0×10^{-6}	1.0×10^{-7}

4.2.4. Application to package alteration at 50 and 30 °C

The calculations up to this point have concerned a package in a geological repository at 90 °C, the temperature for which the GRAAL model parameters were determined, although the values representative of a repository site range from ambient temperature to 50 °C. This is the overpack design reference value, considered as the maximum package temperature at the moment of first contact with water. Having performed the calculations at 90 °C, it is therefore important to apply the GRAAL model to this temperature range.

However, although some parameters of the GRAAL model are accurately known at 50 °C and below (for example, the PRI dissolution rate r_{disso} [12,19], the diffusion coefficient in the PRI D_{PRI} [20], or the silicon concentration at saturation at a given pH [26]), others such as the precipitation parameters are more difficult to determine. The kinetic parameter k' and the threshold value C'_{sat} are inferred from observations of the residual boron release kinetics, provided test results are available over periods sufficiently long for to distinguish between the linear rate due to precipitation and the boron release due to the formation of the PRI. This is the case for the tests at 90 °C but not at lower temperatures because of the slower kinetics. Few extended tests have been conducted above 90 °C, and because of the mechanisms involved in precipitation with significant threshold effects it would be risky to estimate the kinetics below 90 °C by extrapolation from these tests.

For lack of data, it is therefore assumed here that the precipitation kinetics parameter k' between ambient temperature and 90 °C is temperature-dependent according to an Arrhenius law, and three hypothetical values are postulated for the activation energy:

- a central value equal to the activation energy of the diffusion coefficient D_{PRI}, i.e. 86 kJ mol^{-1},
- a minimum value equal to the apparent activation energy measured for the overall residual rate regime and used in the $V_0 \rightarrow V_r$ model, i.e. 53 kJ mol^{-1}, and
- a maximum value of 119 kJ mol^{-1} corresponding to the sum of the central value and the difference between the two preceding values (33 kJ mol^{-1}).

Calculations were performed assuming a 70 cm thick barrier at 50 and 30 °C, for two situations: assuming a notable amount of precipitation in the barrier ($\sigma' = 10^6$ m^{-1}) and disregarding precipitation in the barrier ($\sigma' = 0$). To simplify the calculations, the C'_{sat}/C_{sat} ratio was assumed to be unchanged at 0.95, and the temperature effect on C_{sat} was disregarded by using a single value of 2.0 mol m^{-3}. Table 14 indicates the residual alteration rates with and without precipitation in the barrier. Tables 15 and 16 indicate the durations and altered glass fractions of the transient states for silicon and boron, together with the package lifetime with (Table 15) and without (Table 16) precipitation in the barrier.

In each case the transients are short-lived (no more than 10 years with allowance for precipitation in the barrier, or a 100 years if it is disregarded) for both silicon and boron, and the corresponding altered glass fractions do not exceed 0.01% of the package.

Most of the package alteration therefore occurs under residual rate conditions. The value of r_f is determined at 50 and 30 °C by diffusion in the barrier without precipitation (whereas at 90 °C precipitation at the package/barrier interface determines r_f). With precipitation in the barrier, assuming $\sigma' = 10^6$ m^{-1}, the residual rate approaches the maximum possible value, $r_{disso}(1 - C'_{sat}/C_{sat})$ at 30 °C with a low activation energy for the k' parameter (53 kJ mol^{-1}).

The maximum package lifetime ranges from 53,000 to 160,000 years at 50 °C, and from 190,000 to 700,000 years at 30 °C with allowance for precipitation in the barrier ($\sigma' = 10^6$ m^{-1}). Without precipitation in the barrier, it ranges from 1.1 to 2.1 million years, except at 50 °C with a low activation energy for k' (53 kJ mol^{-1}) where it drops to 470,000 years. The latter case can be compared with the predictions of the $V_0 \rightarrow V_r$ model, which uses a constant residual rate with an activation energy of 53 kJ mol^{-1} and predicts a package lifetime of 31,000 years at 90 °C, 280,000 years at 50 °C and 1.0 million years at 30 °C.

5. Conclusions and outlook

The analytical GRAAL model is a simplification of the hypotheses of the GRAAL model with regard to the secondary phase precipitation equations in the form of a first-order precipitation law for a single siliceous phase. It has been parametered for studying SON68 glass alteration in initially pure water when alteration occurs within a slightly basic pH range (6–9.5) and is dominated by silicon dissolution and precipitation.

The model was compared with the results of 31 laboratory experiments. The comparison is satisfactory with regard to the quantity of altered glass, the alteration kinetics versus the flow rate per unit area, Q/S, and the boron concentration variations in the reactor. The discrepancies observed at high flow rates are explained by the effect of diffusive barrier of the external gel layer, not taken into account in the GRAAL model. The comparison between theoretical and experimental findings shows also discrepancies on the silicon concentrations at equilibrium for different Q/S values; however, that is likely due to the dependency of the silicon concentration at saturation (C_{sat}) on the pH value, not taken into account by the analytical GRAAL model. Namely, the pH values are higher (9–9.5) for lower flow rates, which may lead to differences on the C_{sat} value up to a factor 2–3.

The sensitivity study, performed with regard to the laboratory test results, identified the importance of the kinetic parameters of precipitation of a silicated secondary phase (k' and the precipitation threshold C'_{sat}).

Having validated the analytical GRAAL model in the laboratory, we applied it to the alteration of a SON68 glass package in a geological repository.

Table 14
Final alteration rate: comparison between rates calculated for a finite barrier (r_f) and an infinite barrier (r_{f0}), maximum kinetics (r_{max}) corresponding to $r_{disso}(1 - C'_{sat}/C_{sat})$ and minimum kinetics $r_{diff}(L)$ corresponding to diffusive transport through the barrier. Low, reference and high E_a correspond respectively to 53, 86 and 119 kJ mol^{-1} for the activation energy of the precipitation kinetics parameter k'.

Temperature/parameter	$r_{f0}(\sigma' = 10^6$ m$^{-1})$ [m s^{-1}]	$r_{f0}(\sigma' = 0)$ [m s^{-1}]	$r_{diff}(L)$ [m s^{-1}]	r_{max} [m s^{-1}]	$r_f(\sigma' = 10^6$ m$^{-1})$ [m s^{-1}]	$r_f(\sigma' = 0)$ [m s^{-1}]
90 °C	6.0×10^{-15}	1.0×10^{-15}	3.3×10^{-17}	8.5×10^{-14}	6.0×10^{-15}	1.0×10^{-15}
50 °C, low E_a	1.3×10^{-15}	1.1×10^{-16}	3.3×10^{-17}	3.8×10^{-15}	1.3×10^{-15}	1.4×10^{-16}
50 °C, ref. E_a	7.6×10^{-16}	3.0×10^{-17}	3.3×10^{-17}	3.8×10^{-15}	7.6×10^{-16}	6.2×10^{-17}
50 °C, high E_a	4.3×10^{-16}	7.7×10^{-18}	3.3×10^{-17}	3.8×10^{-15}	4.3×10^{-16}	4.0×10^{-17}
30 °C, low E_a	3.7×10^{-16}	3.0×10^{-17}	3.3×10^{-17}	5.8×10^{-16}	3.7×10^{-16}	6.1×10^{-17}
30 °C, ref. E_a	2.1×10^{-16}	3.6×10^{-18}	3.3×10^{-17}	5.8×10^{-16}	2.1×10^{-16}	3.6×10^{-17}
30 °C, high E_a	9.2×10^{-17}	4.2×10^{-19}	3.3×10^{-17}	5.8×10^{-16}	9.7×10^{-17}	3.3×10^{-17}

Table 15
Duration of transient phases, altered glass fractions, residual rate, and total package lifetime with precipitation in the barrier ($\sigma' = 10^6\ m^{-1}$).

	90 °C	50 °C (53 kJ mol^{-1})	50 °C (86 kJ mol^{-1})	50 °C (119 kJ mol^{-1})	30 °C (53 kJ mol^{-1})	30 °C (86 kJ mol^{-1})	30 °C (119 kJ mol^{-1})
t_{opr} (yrs)	1.5×10^{-5}	7.5×10^{-3}	7.5×10^{-3}	7.5×10^{-3}	3.1×10^{-1}	3.1×10^{-1}	3.1×10^{-1}
t_{Si_stat} (yrs)	3.3×10^{-3}	7.2×10^{-2}	2.0×10^{-1}	6.5×10^{-1}	8.8×10^{-1}	2.7	13
AGF_{Si_stat}	5.8×10^{-7}	2.7×10^{-6}	4.5×10^{-6}	8.1×10^{-6}	9.4×10^{-6}	1.6×10^{-5}	3.6×10^{-5}
t_{PRI} (yrs)	2.7×10^{-1}	1.7×10^{-1}	4.8×10^{-1}	1.5	2.5×10^{-1}	7.6×10^{-1}	3.6
AGF_{PRI}	2.3×10^{-5}	3.2×10^{-6}	5.4×10^{-6}	9.7×10^{-6}	1.4×10^{-6}	2.4×10^{-6}	5.1×10^{-6}
r_f (m s^{-1})	6.0×10^{-15}	1.3×10^{-15}	7.6×10^{-16}	4.3×10^{-16}	3.7×10^{-16}	2.1×10^{-16}	9.7×10^{-17}
Lifetime (yrs)	1.1×10^{4}	5.3×10^{4}	8.9×10^{4}	1.6×10^{5}	1.9×10^{5}	3.2×10^{5}	7.0×10^{5}

Table 16
Duration of transient phases, altered glass fractions, residual rate, and total package lifetime disregarding precipitation in the barrier ($\sigma' = 0$).

	90 °C	50 °C (53 kJ mol^{-1})	50 °C (86 kJ mol^{-1})	50 °C (119 kJ mol^{-1})	30 °C (53 kJ mol^{-1})	30 °C (86 kJ mol^{-1})	30 °C (119 kJ mol^{-1})
t_{opr} (yrs)	1.5×10^{-5}	7.5×10^{-3}	7.5×10^{-3}	7.5×10^{-3}	3.1×10^{-1}	3.1×10^{-1}	3.1×10^{-1}
t_{Si_stat} (yrs)	1.1×10^{-1}	5.7	30	72	32	90	1.1×10^{2}
AGF_{Si_stat}	3.3×10^{-6}	2.4×10^{-5}	5.6×10^{-5}	8.6×10^{-5}	5.6×10^{-5}	9.6×10^{-5}	1.0×10^{-4}
t_{PRI} (yrs)	8.9	14	72	1.7×10^{2}	9.1	26	31
AGF_{PRI}	1.4×10^{-4}	2.9×10^{-5}	6.6×10^{-5}	1.0×10^{-4}	8.2×10^{-6}	1.4×10^{-5}	1.5×10^{-5}
r_f (m s^{-1})	1.0×10^{-15}	1.4×10^{-16}	6.2×10^{-17}	4.0×10^{-17}	6.1×10^{-17}	3.6×10^{-17}	3.3×10^{-17}
Lifetime (yrs)	6.6×10^{4}	4.7×10^{5}	1.1×10^{6}	1.7×10^{6}	1.1×10^{6}	1.9×10^{6}	2.1×10^{6}

In each case of this study, the transients related to the formation of the PRI (boron and alkali release transient) and to its dissolution (silicon transient) were found to be of short duration (not exceeding a few decades to a 100 years) and correspond to very small altered glass fractions (no more than 0.01% of the package mass). The maximum PRI thickness is always less than one micrometer.

The total package lifetime is determined by the residual alteration rate, which is controlled by precipitation of secondary phases in the barrier; the precipitate surface area per unit barrier volume, σ', is a system design basis parameter. For a reasonably high value of $10^6\ m^{-1}$, the package lifetime lies between 200,000 and 700,000 years at 30 °C, depending on the hypothesis used for the temperature-dependence of the precipitation kinetics parameter (an Arrhenius law with an activation energy between 53 and 119 kJ mol^{-1}). For a purely diffusive barrier the package lifetime would have been increased by a factor of 3–6.

This study clearly underscores the importance of the role played by the secondary phase precipitation on the glass durability in the repository. The identification of the phases which could drive the chemical behaviour of silicon, as well as the determination of their properties (composition, solubility, kinetic constants, precipitation surface area) is difficult because of the necessity of taking into account the different solid phases present in the system (metallic corrosion products, argillite), water chemical composition and temperature. Quite a few experimental studies have been undertaken in the last years and are expected to expand the knowledge database in this domain. Last, studies of natural and archaeologic analogues may also contribute to the long term validation of models based on laboratory studies.

Acknowledgements

The authors are grateful to AREVA and the CEA for their financial support of this work. Special thanks are due to Jean-Eric Lartigue for having made accessible and synthetic the otherwise complex experimental database. We are also grateful to P. Jollivet and D. Deneele for allowing us to make use of data from experiments they made or supervised, and for fruitful discussions about the data. We also thank O. Bildstein for providing us data on surface area available for silica precipitation on clay, crucial for proposing a realistic application of the GRAAL model to glass alteration in a geological disposal environment.

Appendix A

Analytical GRAAL model: system of equations, list of characteristic quantities, and solutions for the alteration of initially pristine SON68 glassin a homogenized, initially pure aqueous solution.

A.1. Equations

$$\frac{dE}{dt} = r_{disso}\left(1 - \frac{C_{Si}(t)}{C_{sat}}\right) \tag{A.1}$$

$$\frac{de}{dt} = \frac{r_{hydr}}{1 + \frac{e r_{hydr}}{D_{PRI}}} - \frac{dE}{dt} \tag{A.2}$$

$$\frac{dM_{pr}}{dt} = \rho' k' S'\left(\frac{C_{Si}(t)}{C r_{sat}} - 1\right) \text{ constrained by } M_{pr}(t) \geqslant 0 \tag{A.3}$$

$$\Omega\frac{dC_{Si}}{dt} = SC_{vSi}\frac{dE}{dt} - QC_{Si}(t) - \frac{dM_{pr}}{dt} \tag{A.4}$$

$$\Omega\frac{dC_B}{dt} = SC_{vB}\frac{d(E+e)}{dt} - QC_B(t) \tag{A.5}$$

Initial conditions:

$$E(0) = 0 \tag{A.6}$$

$$e(0) = 0 \tag{A.7}$$

$$M_{pr}(0) = 0 \tag{A.8}$$

$$C_{Si}(0) = 0 \tag{A.9}$$

$$C_B(0) = 0 \tag{A.10}$$

A.2. Characteristic parameters

Note: The input parameters are listed in the Nomenclature given in Section 2.1.

A.2.1. Characteristic times

$t_{kin} = \frac{\Omega C_{sat}}{SC_{vSi} r_{disso}}$: characteristic time for saturation from first-order kinetic law under static conditions, neglecting other phenomena such as precipitation.

$t_{reac} = \Omega/Q$: characteristic residence time of inert elements in the reactor, taking the flow rate into account.

$t_{\text{prec}} = \frac{\Omega C'_{\text{sat}}}{\rho' k' S'}$: characteristic time for precipitation of silicon in the reactor.

t_{c1} given by $t_{c1}^{-1} = t_{\text{kin}}^{-1} + t_{\text{reac}}^{-1}$: characteristic time for the evolution of the silica concentration in the system in the absence of precipitation, taking into account silica saturation and the flow rate.

t_{c2} given by $t_{c1}^{-1} = t_{\text{kin}}^{-1} + t_{\text{reac}}^{-1} + t_{\text{prec}}^{-1}$: characteristic time for the evolution of the silica concentration in the system after the onset of precipitation, taking into account silica saturation and the flow rate.

$t_{\text{opr}} = -t_{c1} \ln\left(1 - \frac{C'_{\text{sat}}}{C_{\text{sat1}}}\right)$: time to the onset of precipitation, if precipitation occurs, under the condition that $C'_{\text{sat}} < C_{\text{sat1}}$ (see Appendix A.2.2 for the definition of C_{sat1}).

$t_{\text{PRI1}} = \frac{D_{\text{PRI}}}{r_{\text{disso}}^2}\left(1 + \frac{SC_{\text{vSi}} r_{\text{disso}}}{QC_{\text{sat}}}\right)^2$: characteristic time for formation of the PRI in the absence of precipitation (see Appendix A.2.3 for the definition of r_{f1}).

$t_{\text{PRI2}} = \frac{D_{\text{PRI}}}{r_{\text{disso}}^2}\left(1 + \frac{SC_{\text{vSi}} r_{\text{disso}} + \rho' k' S'}{QC_{\text{sat}} + \rho' k' S'\left(\frac{C_{\text{sat}}}{C'_{\text{sat}}} - 1\right)}\right)^2$: characteristic time for formation of the PRI in the presence of precipitation (see Appendix A.2.3 for the definition of r_{f2}).

A.2.2. Characteristic concentrations

$C_{\text{sat1}} = C_{\text{sat}} \frac{t_{c1}}{t_{\text{kin}}} = C_{\text{sat}} \frac{SC_{\text{vSi}} r_{\text{disso}}}{SC_{\text{vSi}} r_{\text{disso}} + QC_{\text{sat}}}$: steady-state silica concentration in the reactor in the absence of precipitation, taking into account the effect of the flow rate.

$C_{sat2} = C'_{\text{sat}} + C_{\text{sat}} \frac{t_{c2}}{t_{\text{kin}}}\left(1 - \frac{C'_{\text{sat}}}{C_{\text{sat1}}}\right) = C_{\text{sat}} \frac{t_{c2}}{t_{\text{kin}}} + C'_{\text{sat}} \frac{t_{c2}}{t_{\text{prec}}} = C_{\text{sat}} \frac{SC_{\text{vSi}} r_{\text{disso}} + \rho' k' S'}{SC_{\text{vSi}} r_{\text{disso}} + QC_{\text{sat}} + \rho' k' S' \frac{C_{\text{sat}}}{C'_{\text{sat}}}}$: steady-state silica concentration in the reactor in the presence of precipitation, taking into account the effect of the flow rate.

A.2.3. Characteristic alteration rates

$r_{\text{f1}} = r_{\text{disso}}\left(1 - \frac{C_{\text{sat1}}}{C_{\text{sat}}}\right) = r_{\text{disso}}\left(1 - \frac{t_{c1}}{t_{\text{kin}}}\right) = r_{\text{disso}} \frac{t_{c1}}{t_{\text{reac}}} = r_{\text{disso}} \frac{QC_{\text{sat}}}{SC_{\text{vSi}} r_{\text{disso}} + QC_{\text{sat}}}$: steady-state dissolution rate in the absence of precipitation, taking into account the effect of the flow rate.

$r_{f2} = r_{\text{disso}}\left(1 - \frac{C_{\text{sat2}}}{C_{\text{sat}}}\right) = r_{\text{disso}}\left(1 - \frac{t_{c2}}{t_{\text{kin}}} - \frac{C'_{\text{sat}}}{C_{\text{sat}}}\frac{t_{c2}}{t_{\text{prec}}}\right) = r_{\text{disso}} \frac{QC_{\text{sat}} + \rho' k' S'\left(\frac{C_{\text{sat}}}{C'_{\text{sat}}} - 1\right)}{SC_{\text{vSi}} r_{\text{disso}} + QC_{\text{sat}} + \rho' k' S' \frac{C_{\text{sat}}}{C'_{\text{sat}}}}$: steady-state (final) dissolution rate in the presence of precipitation, taking into account the effect of the flow rate.

A.2.4. Characteristic alteration thicknesses

$E_{c1} = r_{\text{disso}} t_{c1}$: characteristic PRI thickness dissolved under the initial rate regime.

$E_{\text{opr}} = E(t_{\text{opr}}) = E_{c1}\left(\frac{C'_{\text{sat}}}{C_{\text{sat}}} - \left(1 - \frac{C_{\text{sat1}}}{C_{\text{sat}}}\right)\ln\left(1 - \frac{C'_{\text{sat}}}{C_{\text{sat1}}}\right)\right)$: PRI thickness dissolved at the onset of precipitation.

$E_{c2} = r_{\text{disso}}\left(1 - \frac{C'_{\text{sat}}}{C_{\text{sat}}}\right) t_{c2}$: characteristic PRI thickness dissolved under the initial regime after the onset of precipitation.

$\lambda_{\text{PRI1}} = \frac{D_{\text{PRI}}}{r_{f1}} = \frac{D_{\text{PRI}}}{r_{\text{disso}}}\left(1 + \frac{SC_{\text{vSi}} r_{\text{disso}}}{QC_{\text{sat}}}\right)$: characteristic thickness of the PRI in the absence of precipitation.

$\lambda_{\text{PRI2}} = \frac{D_{\text{PRI}}}{r_{f2}} = \frac{D_{\text{PRI}}}{r_{\text{disso}}}\left(1 + \frac{SC_{\text{vSi}} r_{\text{disso}} + \rho' k' S'}{QC_{\text{sat}} + \rho' k' S'\left(\frac{C_{\text{sat}}}{C'_{\text{sat}}} - 1\right)}\right)$: characteristic thickness of the PRI in the presence of precipitation.

A.2.5. Characteristic quantity of precipitate

$M_{\text{pr2}} = \rho' K S'\left(\frac{C_{\text{sat2}}}{C'_{\text{sat}}} - 1\right) t_{c2}$: characteristic quantity of precipitated silica at a time of the order of t_{c2} after the onset of precipitation.

A.3. Solutions and formulas

Time to the onset of precipitation, if precipitation occurs ($C'_{\text{sat}} > C_{\text{sat1}}$):

$$t_{\text{opr}} = -t_{c1} \ln\left(1 - \frac{C'_{\text{sat}}}{C_{\text{sat1}}}\right) \tag{A.11}$$

Dissolution rate of the PRI (before and after the onset of precipitation):

$$r_{\text{Si}}(t) = \frac{dE}{dt} = r_{f1} + (r_{\text{disso}} - r_{\text{f1}}) e^{-\frac{t}{t_{c1}}} \tag{A.12}$$

$$\text{or } r_{f2} + \left(r_{\text{disso}}\left(1 - \frac{C'_{\text{sat}}}{C_{\text{sat}}}\right) - r_{f2}\right) e^{-\frac{t - t_{\text{opr}}}{t_{c2}}} \tag{A.13}$$

Silicon concentrations (before and after the onset of precipitation):

$$C_{\text{Si}}(t) = C_{\text{sat1}}\left(1 - e^{-\frac{t}{t_{c1}}}\right) \tag{A.14}$$

$$\text{or } C_{\text{sat2}}\left(1 - \left(1 - \frac{C'_{\text{sat}}}{C_{\text{sat2}}}\right) e^{-\frac{t - t_{\text{opr}}}{t_{c2}}}\right) \tag{A.15}$$

Boron concentrations:

$$C_B(t) = C_{\text{Bdiss}}(t) + C_{\text{B\_PRI}}(t) \tag{A.16}$$

Boron component from the dissolved PRI (before and after the onset of precipitation):

$$C_{\text{Bdiss}}(t) = \frac{C_{\text{vB}}}{C_{\text{vSi}}} C_{\text{Si}}(t) \tag{A.17}$$

or

$$C_{\text{Bdiss}}(t) = \frac{C_{\text{vB}}}{C_{\text{vSi}}} C'_{\text{sat}} e^{-\frac{t - t_{\text{opr}}}{t_{\text{reac}}}} + \frac{SC_{\text{vB}}}{\Omega}\left(r_{f2} t_{\text{reac}}\left(1 - e^{-\frac{t - t_{\text{opr}}}{t_{\text{reac}}}}\right) + \left(r_{\text{disso}}\left(1 - \frac{C'_{\text{sat}}}{C_{\text{sat}}}\right) - r_{f2}\right) \frac{t_{\text{kin}} t_{\text{prec}}}{t_{\text{kin}} + t_{\text{prec}}}\left(e^{-\frac{t - t_{\text{opr}}}{t_{\text{reac}}}} - e^{-\frac{t - t_{\text{opr}}}{t_{c2}}}\right)\right) \tag{A.18}$$

Boron component from the current PRI:

$$C_{\text{B\_PRI}}(t) = \frac{SC_{\text{vB}}}{\Omega} \frac{D_{\text{PRI}}}{r_{\text{Si}}(t)} I(H(t), U(t), \Lambda(t)) \tag{A.19}$$

where

$$I(H, U, \Lambda) = e^{-\Lambda H} \sum_{n \geqslant 0} \frac{\Lambda^n}{n!} \frac{U^{n+1-\Lambda} H^{\Lambda} - H^{n+1}}{n + 1 - \Lambda}$$

$$H(t) = 1 - k(t); U(t) = 1 - \frac{r_{\text{Si}}(t)}{r_{\text{hydr}}}; \Lambda(t) = \frac{D_{\text{PRI}}}{t_{\text{reac}} (r_{\text{Si}}(t))^2}$$

$k(t)$ verifies : $-k - \ln(1 - k)$

$$= \frac{t (r_{\text{Si}}(t))^2}{D_{\text{PRI}}} - \frac{r_{\text{Si}}(t)}{r_{\text{hydr}}} - \ln\left(1 - \frac{r_{\text{Si}}(t)}{r_{\text{hydr}}}\right) \tag{A.20}$$

Back-of-the-envelope expression:

$$C_{\text{B\_PRI}}(t) = \frac{SC_{\text{vB}} D_{\text{PRI}}}{\Omega}\left(\frac{k(t)}{r_{\text{Si}}(t)} - \frac{k(t_1)}{r_{\text{Si}}(t_1)}\right) \quad \text{where } t_1 = \max(t - t_{\text{reac}}; 0) \tag{A.21}$$

Total altered glass thickness

$$E_{\text{tot}}(t) = r_{f1} t + (r_{\text{disso}} - r_{\text{f1}}) t_{c1}\left(1 - e^{-\frac{t}{t_{c1}}}\right) + D_{\text{PRI}}\left(\frac{k(t)}{r_{\text{Si}}(t)} - \frac{1}{r_{\text{hydr}}}\right) \tag{A.22}$$

or

$$E_{tot}(t) = E_{opr} + r_{f2}(t - t_{opr}) + \left(r_{disso}\left(1 - \frac{C'_{sat}}{C_{sat}}\right) - r_{f2}\right) t_{c2}\left(1 - e^{-\frac{t-t_{opr}}{t_{c2}}}\right) + D_{PRI}\left(\frac{k(t)}{r_{Si}(t)} - \frac{1}{r_{hydr}}\right) \quad (A.23)$$

$$E_{opr} = r_{disso} t_{c1}\left(\frac{C'_{sat}}{C_{sat}} - \left(1 - \frac{C_{sat1}}{C_{sat}}\right)\ln\left(1 - \frac{C'_{sat}}{C_{sat1}}\right)\right) \quad (A.24)$$

Total glass alteration rate:

$$r_{tot}(t) = \frac{dE_{tot}}{dt} = \frac{r_{Si}(t)}{k(t)} \quad (A.25)$$

Total altered glass mass, according to the shrinking core model:

$$M_{tot}(t) = M_{init}\left(1 - \left(1 - \frac{\rho_{glass} S E_{tot}(t)}{3M_{init}}\right)^3\right) \quad (A.26)$$

Appendix B

Analytical GRAAL model: System of equations, list of characteristic quantities, and solutions for the alteration of initially pristine SON68 glassin initially pure water in the presence of a diffusion barrier.

B.1. Equations

The following equations are similar to Eqs. (1)–(5) given for a homogeneous solution (Section 2.2), and are adapted to a barrier described as a 1D Cartesian diffusive medium. They are the equations concerning silicon:

$$\frac{dE}{dt} = r_{disso}\left(1 - \frac{C_{Si}(0,t)}{C_{sat}}\right) \quad (B.1)$$

$$\frac{\partial m_{pr}(z,t)}{\partial t} = \rho' k' \sigma'\left(\frac{C_{Si}(z,t)}{C'_{sat}} - 1\right) \quad \text{if } m_{pr}(z,t) > 0 \quad \text{or} \quad C_{Si}(z,t) > C'_{sat};\ 0 \text{ otherwise} \quad (B.2)$$

$$\frac{\partial M_{pr}(0,t)}{\partial t} = \rho' k' S'\left(\frac{C_{Si}(0,t)}{C'_{sat}} - 1\right) \quad \text{if } M_{pr}(0,t) > 0 \quad \text{or} \quad C_{Si}(0,t) > C'_{sat};\ 0 \text{ otherwise} \quad (B.3)$$

$$\omega \frac{\partial C_{Si}}{\partial t}(z,t) = D_{barr}\frac{\partial^2 C_{Si}}{\partial z^2}(z,t) - \frac{\partial m_{pr}}{\partial t}(z,t) \quad (B.4)$$

$$\Omega \frac{\partial C_{Si}}{\partial t}(0,t) = SC_{vSi}\frac{dE}{dt} + \Sigma D_{barr}\frac{\partial C_{Si}}{\partial z}(0,t) - \frac{\partial M_{pr}}{\partial t}(0,t) \quad (B.5)$$

The initial and boundary conditions for silicon are:

$$C_{Si}(z,0) = 0 \quad (B.6)$$

$$C_{Si}(L,t) = 0 \quad (B.7)$$

- Eq. (B.1) expressing silicon first-order law is an adaptation of Eq. (1) at the glass/barrier interface.
- Eqs. (B.2) and (B.3) express the silicon precipitation, respectively inside the barrier ($m_{pr}(z,t)$) and at the glass/barrier interface ($M_{pr}(0,t)$).
- Eq. (B.4) is the silicon diffusion equation in the barrier.
- Eq. (B.5) is the flow expression for silicon at the glass/barrier interface. Note that the free volume of water at this interface, Ω, can be assumed to tend toward zero.
- The equation expressing the total altered glass thickness is:

$$\frac{de}{dt} = \frac{r_{hydr}}{1 + \frac{e r_{hydr}}{D_{PRI}}} - \frac{dE}{dt} \quad (B.8)$$

The equations concerning boron concern its transport and are as follows:

$$\omega \frac{\partial C_B}{\partial t} = D_{barr}\frac{\partial^2 C_B}{\partial z^2} \quad (B.9)$$

$$\Omega \frac{\partial C_B}{\partial t}(0,t) = SC_{vSi}\frac{d(E+e)}{dt} + \Sigma D_{barr}\frac{\partial C_B}{\partial z}(0,t) \quad (B.10)$$

The initial conditions and outer boundary conditions for boron are:

$$C_B(z,0) = 0 \quad (B.11)$$

$$C_B(L,t) = 0 \quad (B.12)$$

B.2. Characteristic parameters of the system

$t_{pbarr} = \frac{\omega L^2}{\pi D_{barr}}$: diffusion time through the barrier,

$t_{ibarr1} = \frac{\omega D_{barr}}{\pi r_{disso}^2}\left(\frac{\Sigma C_{sat}}{SC_{vSi}}\right)^2 = \frac{\omega \delta_1^2}{\pi D_{barr}}$: characteristic time of inflexion of glass alteration rate due to silicon diffusion in the barrier, in the absence of precipitation,

$t_{ibarr2} = \frac{\omega D_{barr}}{\pi}\left(\frac{\Sigma C_{sat}}{SC_{vSi} r_{disso} + \rho' k' S' \frac{C_{sat}}{C'_{sat}}}\right)^2 = \frac{\omega \delta_2^2}{\pi D_{barr}}$: characteristic time of inflexion of glass alteration rate due to silicon diffusion in the barrier, taking into account the precipitation at the glass/barrier interface,

$t_{opr} = \frac{\omega D_{barr}}{\pi r_{disso}^2}\left(\frac{\Sigma C'_{sat}}{SC_{vSi}}\frac{1}{1 - \frac{C'_{sat}}{C_{sat}}}\right)^2 = \frac{t_{ibarr1}}{\left(\frac{C_{sat}}{C'_{sat}} - 1\right)^2}$: time to onset of precipitation,

$t'_{i2} = \frac{1+p'}{p'^2} t_{opr}$: auxiliary time for describing the decrease of the glass alteration rate in the presence of precipitation in the barrier (p' defined below),

$t_{prec\_barr} = \frac{\omega C_{sat}}{\rho' k' \sigma'}$: characteristic time of precipitation of the silicon in the barrier,

$t_{PRI} = \frac{D_{PRI}}{r_f^2}$; $\lambda_{PRI} = \frac{D_{PRI}}{r_f}$: characteristic time of formation, characteristic thickness of the PRI (r_f defined below),

$\delta_1 = \frac{\Sigma D_{barr} C_{sat}}{SC_{vSi} r_{disso}}$: characteristic length of diffusion of the silicon in the barrier in the absence of precipitation,

$\delta_2 = \frac{\Sigma D_{barr} C_{sat}}{SC_{vSi} r_{disso} + \rho' k' S' \frac{C_{sat}}{C'_{sat}}}$: characteristic length of diffusion of the silicon in the barrier, taking into account the precipitation at the glass/barrier interface,

$\delta'_0 = \frac{1}{W'_0} = \left(\frac{C_{sat} D_{barr}}{\rho' k' \sigma'}\right)^{1/2}$: characteristic length of the precipitation layer in the barrier under steady-state conditions, $p' = \frac{\delta_2}{\delta'_0} = \left(\frac{\rho' k' \sigma'}{C_{sat} D_{barr}}\right)^{1/2} \frac{\Sigma D_{barr} C_{sat}}{SC_{vSi} r_{disso} + \rho' k' S' \frac{C_{sat}}{C'_{sat}}}$: Ratio of characteristic lengths of diffusion to precipitation in the barrier, indicative of the importance of the precipitation phenomenon,

$r_f = r_{disso}\left(1 - \frac{C'_{sat}}{C_{sat}}\frac{1 + F - \left((Fp')^2 + \frac{\delta_2^2}{L^2}(1-p'^2)\right)^{1/2} - p'^2}{1 - p'^2}\right)$, where $F = \left(\frac{t_{ibarr2}}{t_{opr}}\right)^{1/2} = \frac{\delta_2}{\delta_1}\left(\frac{C_{sat}}{C'_{sat}} - 1\right) = \frac{SC_{vSi} r_{disso}\left(\frac{C_{sat}}{C'_{sat}} - 1\right)}{SC_{vSi} r_{disso} + \rho' k' S' \frac{C_{sat}}{C'_{sat}}}$: final rate, taking account diffusion and precipitation in the barrier and around the glass block, for a finite barrier,

$r_{f0} = r_{disso}\left(1 - \frac{C'_{sat}}{C_{sat}}\frac{1+F+p'}{1+p'}\right) = r_{disso}\left(1 - \frac{C'_{sat}}{C_{sat}}\right)\Theta$, where $\Theta = \frac{\rho' k' S' \frac{C_{sat}}{C'_{sat}} + \left(\rho' k' \sigma' D_{barr} C_{sat}\right)^{1/2} \Sigma}{SC_{vSi} r_{disso} + \rho' k' S' \frac{C_{sat}}{C'_{sat}} + \left(\rho' k' \sigma' D_{barr} C_{sat}\right)^{1/2} \Sigma}$: final rate, taking account diffusion and precipitation in the barrier and around the glass block, for an infinite barrier,

$r_{d1} = r_{disso}\frac{C'_{sat}}{C_{sat}}\frac{Fp'}{1+p'}$: auxiliary alteration rate for describing the decrease of the glass alteration rate in the presence of precipitation in the barrier.

B.3. Transformation and solution of the equations

The solution of the equations mainly concerns those regarding silicon ((B.1)–(B.7)) because the primary objective of the sensitivity study concerning the repository is to predict the quantity of altered glass resulting from equations ((B.8), determined on the basis of Eqs. (B.1)–(B.7)).

The expressions for Eqs. (B.1)–(B.7) reveal that the time to the onset of precipitation (t_{opr}) corresponds to the time necessary to reach C'_{sat} at the glass/barrier interface. The system is thus reduced to the following:

$$\omega\frac{\partial C_{Si}}{\partial t}(z,t) = D_{barr}\frac{\partial^2 C_{Si}}{\partial z^2}(z,t) \tag{B.13}$$

$$SC_{vSi}r_{disso}\left(1-\frac{C_{Si}(0,t)}{C_{sat}}\right) = -\Sigma D_{barr}\frac{\partial C_{Si}}{\partial z}(0,t) \tag{B.14}$$

$$C_{Si}(z,0) = 0 \tag{B.15}$$

$$C_{Si}(L,t) = 0 \tag{B.16}$$

$$C_{Si}(0,t_{opr}) = C'_{sat} \tag{B.17}$$

Precipitation is initiated when C'_{sat} is reached at the glass/barrier interface, i.e. for $t = t_{opr}$, the silicon concentration profile in the barrier is designated $C_{Si\_opr}(z)$. A precipitation front designated $z_{pr}(t)$ is subsequently established in the barrier, and equations ((B.1)–(B.7)) become:

$$SC_{vSi}r_{disso}\left(1-\frac{C_{Si}(0,t)}{C_{sat}}\right) = -\Sigma D_{barr}\frac{\partial C_{Si}}{\partial z}(0,t) + \rho' k' S'\left(\frac{C_{Si}(0,t)}{C'_{sat}}-1\right) \tag{B.18}$$

$$\omega\frac{\partial C_{Si}}{\partial t}(z,t) = D_{barr}\frac{\partial^2 C_{Si}}{\partial z^2}(z,t) - \rho' k'\sigma'\left(\frac{C_{Si}(z,t)}{C'_{sat}}-1\right) \quad \text{for } z < z_{pr}(t) \tag{B.19}$$

$$C_{Si}(z_{pr}(t),t) = C'_{sat} \tag{B.20}$$

$$\frac{\partial C_{Si}}{\partial z}\left(z^+_{pr}(t),t\right) = \frac{\partial C_{Si}}{\partial z}\left(z^-_{pr}(t),t\right) \tag{B.21}$$

$$\omega\frac{\partial C_{Si}}{\partial t}(z,t) = D_{barr}\frac{\partial^2 C_{Si}}{\partial z^2}(z,t), \quad \text{for } z > z_{pr}(t) \tag{B.22}$$

$$C_{Si}(L,t) = 0 \tag{B.23}$$

$$C_{Si}(z,t_{opr}) = C_{Si\_opr}(z) \tag{B.24}$$

The dissolved PRI thickness is given by the following equation:

$$\frac{dE}{dt} = r_{disso}\left(1-\frac{C_{Si}(0,t)}{C_{sat}}\right) \tag{B.25}$$

The equation system (B.18)–(B.24) can be solved by assuming steady-state conditions for a given thickness $l(t)$ corresponding to the diffusion depth in the barrier, until the final thickness, L, is reached after a time corresponding to the diffusion time through the barrier: $t_{pbarr} = \frac{\omega L^2}{\pi D_{barr}}$. After calculating the steady-state conditions for long time periods (Appendix B.3.1), this approximate calculation is discussed in Appendix B.3.2.

B.3.1. Steady-State conditions for extended time periods ($t > t_{pbarr}$)

Steady-state conditions are defined by the following equations, where $C(t)$ is the silicon concentration for long durations and z_{pr} the position of the precipitation front:

$$SC_{vSi}r_{disso}\left(1-\frac{C(0)}{C_{sat}}\right) = -\Sigma D_{barr}\frac{dC}{dz}(0) + \rho' k' S'\left(\frac{C(0)}{C'_{sat}}-1\right) \tag{B.26}$$

$$D_{barr}\frac{d^2C}{dz^2}(z) = \rho' k'\sigma'\left(\frac{C(z)}{C'_{sat}}-1\right) \quad \text{for } z < z_{pr} \tag{B.27}$$

$$\frac{dC}{dz}\left(z^+_{pr}\right) = \frac{dC}{dz}\left(z^-_{pr}\right) \tag{B.28}$$

$$C(z) = C'_{sat}\frac{L-z}{L-z_{pr}}, \quad \text{for } z > z_{pr} \tag{B.29}$$

The concentration condition (B.29) and flow condition (B.28) at the precipitation front are defined to solve Eq. (B.27) and to express the concentration $C(z)$ as a function of z_{pr} for $z < z_{pr}$:

$$C(z) = C'_{sat}\left(1+\frac{\sinh\left(W'_0(z_{pr}-z)\right)}{W'_0(L-z_{pr})}\right) \tag{B.30}$$

where $W'_0 = \left(\frac{\rho' k'\sigma'}{C_{sat}D_{barr}}\right)^{1/2}$ and sinh is the hyperbolic sine function.

The z_{pr} value is then calculated by applying the boundary condition (B.26) at the glass/barrier interface. It is given by the following equation:

$$\frac{\left(\rho' k' S' + SC_{vSi}r_{disso}\frac{C'_{sat}}{C_{sat}}\right)\sinh\left(W'_0 z_{pr}\right) + \Sigma D_{barr}C'_{sat}W'_0\cosh\left(W'_0 z_{pr}\right)}{W'_0(L-z_{pr})} = SC_{vSi}r_{disso}\left(1-\frac{C'_{sat}}{C_{sat}}\right) \tag{B.31}$$

The PRI dissolution rate is then determined by the relation:

$$\frac{dE}{dt} = r_{disso}\left(1-\frac{C'_{sat}}{C_{sat}}\left(1+\frac{\sinh\left(W'_0 z_{pr}\right)}{W'_0(L-z_{pr})}\right)\right) \tag{B.32}$$

B.3.2. Quasi-Steady state conditions before barrier breakthrough ($t < t_{pbarr}$)

For shorter time periods the equation system (B.18)–(B.24) can be solved by approximation by assuming a quasi-steady state diffusion profile to the diffusion depth in the barrier $l(t) = \left(\frac{\pi D_{barr}t}{\omega}\right)^{1/2}$ in which the silicon concentration is assumed equal to zero. The silicon profile is then linearized between $z_{pr}(t)$ (precipitation front in the barrier) and $l(t)$. This gives equations similar to (B.26)–(B.29) in which $l(t)$ is substituted for L. The value of $z_{pr}(t)$ is given by:

$$\frac{\left(\rho' k' S' + SC_{vSi}r_{disso}\frac{C'_{sat}}{C_{sat}}\right)\sinh\left(W'_0 z_{pr}(t)\right) + \Sigma D_{barr}C'_{sat}W'_0\cosh\left(W'_0 z_{pr}(t)\right)}{W'_0(l(t)-z_{pr}(t))} = SC_{vSi}r_{disso}\left(1-\frac{C'_{sat}}{C_{sat}}\right) \tag{B.33}$$

and the PRI dissolution rate is then determined by the relation:

$$\frac{dE}{dt} = r_{disso}\left(1-\frac{C'_{sat}}{C_{sat}}\left(1+\frac{\sinh\left(W'_0 z_{pr}(t)\right)}{W'_0(l(t)-z_{pr}(t))}\right)\right) \tag{B.34}$$

B.3.3. Dissolution conditions before precipitation: justification of the approximation for quasi-steady state conditions for short time periods

The first alteration regime prior to the onset of precipitation ($t < t_{opr}$) is determined by solving the system of Eqs. (B.13)–(B.17),

giving exact analytical expressions that can be compared directly with the expressions obtained by approximating semi-steady state conditions. It can demonstrated that for a barrier of infinite thickness (i.e. for a time $t \ll t_{pbarr}$), the PRI dissolution rate is given by the following expression:

$$r_{Si\_exact}(t) = \frac{dE}{dt} = r_{disso} e^{\frac{t}{\pi t_{ibarr1}}} \mathrm{erfc}\left(\left(\frac{t}{\pi t_{ibarr1}}\right)^{1/2}\right) \tag{B.35}$$

where $\mathrm{erfc}(z) = \frac{2}{\pi^{1/2}} \int_z^{+\infty} e^{-y^2}\, dy$ is the complementary error function.

The rate obtained with the approximation of quasi-steady state conditions is calculated from Eq. (B.14) by postulating that $\frac{\partial C_{Si}}{\partial z}(0,t) = \frac{C_{Si}(0,t)}{l(t)}$. Hence:

$$r_{Si\_approx}(t) = \frac{dE}{dt} = r_{disso} \frac{\Sigma D_{barr} C_{sat}}{\Sigma D_{barr} C_{sat} + S C_{vSi} r_{disso} \left(\frac{\pi D_{barr} t}{\omega}\right)^{1/2}} = \frac{r_{disso}}{1 + \left(\frac{t}{t_{ibarr1}}\right)^{1/2}} \tag{B.36}$$

It can then be demonstrated that $\frac{2(1+\tau^{1/2})}{\tau^{1/2}+(\tau+2\pi)^{1/2}} \leqslant \frac{r_{Si\_exact}(\tau)}{r_{Si\_approx}(\tau)} \leqslant \frac{2(1+\tau^{1/2})}{\tau^{1/2}+(\tau+4)^{1/2}}$, where $\tau = \frac{t}{t_{ibarr1}}$. The ratio between the two rates is therefore between 0.8 and 1.25.

Moreover, for high τ values the ratio $r_{Si\_exact}(\tau)/r_{Si\_approx}(\tau)$ is very near $1 + \tau^{-1/2}$, or about 1.05 at the onset of precipitation ($t = t_{opr}$), whereas the rate has dropped by a factor of 20 (based on the reference values of the C'_{sat}/C_{sat} ratio). This justifies the approximation of steady-state conditions, as well as the following expression for the time to the onset of precipitation:

$$t_{opr} = \frac{t_{ibarr1}}{\left(\frac{C_{sat}}{C'_{sat}} - 1\right)^2} \tag{B.37}$$

After the onset of precipitation, the diffusion front progresses at a lower rate and the approximation of quasi-steady state conditions is amply justified unless precipitation results in a shorter characteristic time. The characteristic time of precipitation in the barrier given by $t_{prec\_barr} = \frac{\omega C_{sat}}{\rho' k' \sigma'}$ is no less than about 1 day, even for very high σ' values ($10^8\ m^{-1}$). It is always much longer than the inflexion time t_{ibarr1}.

B.3.4. Calculating the precipitation front $z_{pr}(t)$ and the PRI dissolution rate

Eq. (B.33) can be written as follows:

$$\frac{\sinh\left(W'_0 z_{pr}(t)\right) + \delta_2 W'_0 \cosh\left(W'_0 z_{pr}(t)\right)}{W'_0 (l(t) - z_{pr}(t))} = F \tag{B.38}$$

where

$$F = \frac{S C_{vSi} r_{disso} \left(\frac{C_{sat}}{C'_{sat}} - 1\right)}{S C_{vSi} r_{disso} + \rho' k' S' \frac{C_{sat}}{C'_{sat}}}$$

and

$$\delta_2 = \frac{\Sigma D_{barr} C_{sat}}{S C_{vSi} r_{disso} + \rho' k' S' \frac{C_{sat}}{C'_{sat}}}$$

The precipitation front $z_{pr}(t)$ can be calculated from the following expression derived from relation (B.38):

$$z_{pr}(t) = \frac{1}{W'_0} \ln \frac{F W'_0 (l(t) - z_{pr}(t)) + \left(\left(F W'_0 (l(t) - z_{pr}(t))\right)^2 + 1 - \delta_2^2 W'^2_0\right)^{1/2}}{1 + \delta_2 W'_0} \tag{B.39}$$

Relation (B.39) can be used to calculate $z_{pr}(t)$ by iteration from an initial zero value. It is valid provided $\left(F W'_0 l(t)\right)^2 + 1 - \delta_2^2 W'^2_0 \geqslant \left(1 + \delta_2 W'_0 - F W'_0 l(t)\right)^2$, which is equivalent to $F l(t) \geqslant \delta_2$, or in other words, $l(t) \geqslant \frac{\delta_1 C'_{sat}}{C_{sat} - C'_{sat}}$. This corresponds to the onset threshold of precipitation given by relation (B.37).

Relation (B.39) can be written with the $z_{pr}(t)/\delta_2$ ratio verifying ($p' = \delta_2 W'_0$):

$$\frac{z_{pr}(t)}{\delta_2} = \frac{1}{p'} \ln \frac{F p' \left(\left(\frac{t}{t_{ibarr2}}\right)^{1/2} - \frac{z_{pr}(t)}{\delta_2}\right) + \left(\left(F_{p'}\left(\left(\frac{t}{t_{ibarr2}}\right)^{1/2} - \frac{z_{pr}(t)}{\delta_2}\right)\right)^2 + 1 - p'^2\right)^{1/2}}{1 + p'} \tag{B.40}$$

The PRI dissolution rate calculated from relation (B.34) is given by:

$$r_{Si}(t) = \frac{dE}{dt} = r_{disso} \left(1 - \frac{C'_{sat}}{C_{sat}} \frac{1 + F - \left((F_{p'})^2 + \frac{\delta_2^2 (1 - p'^2)}{(l(t) - z_{pr}(t))^2}\right)^{1/2} - p'^2}{1 - p'^2}\right) \tag{B.41}$$

B.4. Formulas

B.4.1. PRI dissolution rate

For $t < t_{opr}$:

$$r_{Si}(t) = \frac{dE}{dt} = r_{disso} \frac{\Sigma D_{barr} C_{sat}}{\Sigma D_{barr} C_{sat} + S C_{vSi} r_{disso} \left(\frac{\pi D_{barr} t}{\omega}\right)^{1/2}} = \frac{r_{disso}}{1 + \left(\frac{t}{t_{ibarr1}}\right)^{1/2}} \tag{B.42}$$

For $t_{opr} < t < t_{pbarr}$, if it is assumed that $z_{pr}(t)$ is small compared with $l(t)$, which is justified as long as C'_{sat}/C_{sat} is near 1, then $l(t)$ can be substituted for $l(t) - z_{pr}(t)$ in relation (B.41) to obtain an analytically integrable expression:

$$r_{Si}(t) = \frac{dE}{dt} \approx r_{disso} \left(1 - \frac{C'_{sat}}{C_{sat}} \frac{1 + F - \left((Fp')^2 + (1 - p'^2) \frac{t_{ibarr2}}{t}\right)^{1/2} - p'^2}{1 - p'^2}\right) \tag{B.43}$$

$$r_{Si}(t) \approx r_{f0} + \frac{r_{d1}}{1 - p'} \left(\left(1 + (1 - p') \frac{t'_{i2}}{t}\right)^{1/2} - 1\right) \tag{B.44}$$

where

$$r_{f0} = r_{disso} \left(1 - \frac{C'_{sat}}{C_{sat}} \frac{1 + F + p\prime}{1 + p'}\right); \quad r_{d1} = r_{disso} \frac{C'_{sat}}{C_{sat}} \frac{Fp'}{1 + p'};$$

$$t'_{i2} = \frac{1 + p'}{F^2 p'^2} t_{ibarr2} = \frac{1 + p'}{p'^2} t_{opr}$$

and

$$F = \left(\frac{t_{ibarr2}}{t_{opr}}\right)^{1/2} = \frac{\delta_2}{\delta_1} \left(\frac{C_{sat}}{C'_{sat}} - 1\right) = \frac{S C_{vSi} r_{disso} \left(\frac{C_{sat}}{C'_{sat}} - 1\right)}{S C_{vSi} r_{disso} + \rho' k' S' \frac{C_{sat}}{C'_{sat}}}$$

For $t > t_{pbarr}$:

$$r_{Si}(t) = \frac{dE}{dt} \approx r_{disso} \left(1 - \frac{C'_{sat}}{C_{sat}} \frac{1 + F - \left((Fp')^2 + \frac{\delta_2^2}{L^2}(1 - p'^2)\right)^{1/2} - p'^2}{1 - p'^2}\right) = r_f \tag{B.45}$$

B.4.2. PRI thickness

$$e(t) \approx \frac{D_{PRI} k(t)}{r_{Si}(t)} - \frac{D_{PRI}}{r_{hydr}} \tag{B.46}$$

where $k(t)$ is given by:

$$-k - \ln(1-k) = \frac{t(r_{Si}(t))^2}{D_{PRI}} - \frac{r_{Si}(t)}{r_{hydr}} - \ln\left(1 - \frac{r_{Si}(t)}{r_{hydr}}\right) \quad (B.47)$$

B.4.3. Dissolved PRI thickness

For $t < t_{opr}$:

$$E(t) = 2r_{disso}t_{ibarr1}\left(\left(\frac{t}{t_{ibarr1}}\right)^{1/2} - \ln\left(1 + \left(\frac{t}{t_{ibarr1}}\right)^{1/2}\right)\right) \quad (B.48)$$

For $t_{opr} < t < t_{pbarr}$:

$$E(t) = E(t_{opr}) + r_{f0}(t - t_{opr}) + r_{d1}I(t) \quad (B.49)$$

where

$$I(t) = \int_{t_{opr}}^{t} \frac{\left(1 + (1-p')\frac{t'_{i2}}{t'}\right)^{1/2} - 1}{1-p'} dt' = 2t'_{i2}\int_{\left(\frac{t_{opr}}{t'_{i2}}\right)^{1/2}}^{\left(\frac{t}{t'_{i2}}\right)^{1/2}} \frac{(v^2 + 1 - p')^{1/2} - v}{1-p'} dv \quad (B.50)$$

Finally:

$$E(t) = E(t_{opr}) + E_{add}(t) - E_{add}(t_{opr}) \quad (B.51)$$

where

$$E_{add}(t) = r_{f0}t + r_{d1}\left(\frac{-t + \left(t\left(t + (1-p')t'_{i2}\right)\right)^{1/2}}{1-p'} + t'_{i2}\ln\frac{t^{1/2} + \left(t + (1-p')t'_{i2}\right)^{1/2}}{t'^{1/2}_{i2}}\right) \quad (B.52)$$

For $t > t_{pbarr}$:

$$E(t) = E(t_{pbarr}) + r_f(t - t_{pbarr}) \quad (B.53)$$

B.4.4. Glass alteration rate

$$r_{tot}(t) = \frac{dE_{tot}}{dt} = \frac{r_{Si}(t)}{k(t)} \quad (B.54)$$

References

[1] N. Jacquet-Francillon, R. Bonniaud, C. Sombret, Radiochimica Acta 25 (1978) 231–240.
[2] Assemblée Nationale, Loi no. 2006-739 du 28/06/2006 de programme relative à la gestion des matières et des déchets radioactifs. <www.legifrance.gouv.fr>.
[3] ANDRA, Dossier 2005 Argile, Tome "Phenomenological Evolution of a Geological Repository", ANDRA Report C.RP.ADS.04.0025, 2005, pp. 1–525.
[4] R.C. Ewing, Natural glasses: analogues for radioactive waste forms, in: G.J. McCarthy (Ed.), MRS Symposium – Scientific Basis for Nuclear Waste Management, vol. 1, 1979, pp. 57–66.
[5] A. Verney-Carron, S. Gin, G. Libourel, Geochimica et Cosmochimica Acta 72 (2008) 5372–5385.
[6] A. Verney-Carron, S. Gin, P. Frugier, G. Libourel, Geochimica et Cosmochimica Acta 74 (2010) 2291–2315.
[7] P. van Iseghem, K. Lemmens, M. Aertsens, S. Gin, I. Ribet, B. Grambow, J.L. Crovisier, M. Del Nero, E. Curti, B. Schwyn, B. Luckscheiter, T. McMenamin, Chemical durability of high-level waste glass in repository environment: main conclusions and remaining uncertainties from the GLASTAB and GLAMOR projects, in: MRS Symposium – Scientific Basis for Nuclear Waste Management XXIX, vol. 932, 2006, pp. 293–304.
[8] P. Frugier, S. Gin, Y. Minet, T. Chave, B. Bonin, N. Godon, J.E. Lartigue, P. Jollivet, A. Ayral, L. De Windt, G. Santarini, Journal of Nuclear Materials 380 (2008) 8–21.
[9] P. Frugier, T. Chave, S. Gin, J.E. Lartigue, Journal of Nuclear Materials 392 (2009) 552–567.
[10] C. Cailleteau, F. Angeli, F. Devreux, S. Gin, J. Jestin, P. Jollivet, O. Spalla, Nature Materials 7 (2008) 978–983.
[11] P. Jollivet, F. Angeli, C. Cailleteau, F. Devreux, P. Frugier, S. Gin, Journal of Non-Crystalline Solids 354 (2008) 4952–4958.
[12] B. Grambow, A general rate equation for nuclear waste glass corrosion, in: C.M. Jantzen, J.A. Stone, R.C. Ewing (Eds.), MRS Symposium – Scientific Basis for Nuclear Waste Management VII, vol. 44, 1985, pp. 15–27.
[13] B. Grambow, R. Muller, Journal of Nuclear Materials 298 (2001) 112–124.
[14] N. Rajmohan, P. Frugier, S. Gin, Modeling the passivating layer of nuclear waste glasses: 1. Experimental observations, Chemical Geology, accepted for publication.
[15] I. Ribet, S. Gin, E. Vernaz, R. Do Quang, Long-term behavior of nuclear glass: the r(t) operational model, in: GLOBAL 2001, Paris, 2001, pp. 1–9.
[16] I. Ribet, S. Bétrémieux, S. Gin, F. Angeli, C. Jégou, Long-term behavior of vitrified waste packages, in: GLOBAL 2009, Paris, 2009.
[17] J.D. Rimstidt, H.L. Barnes, Geochimica et Cosmochimica Acta 44 (1980) 1683–1699.
[18] G. Geneste, F. Bouyer, S. Gin, Journal of Non-Crystalline Solids 352 (2006) 3147–3152.
[19] T. Advocat, J.L. Crovisier, E. Vernaz, G. Ehret, H. Charpentier, Hydrolysis of R7T7 nuclear waste glass in dilute media: mechanisms and rate as a function of pH, in: T.A. Abrajano Jr., L.H. Johnson (Eds.), MRS Symposium – Scientific Basis for Nuclear Waste Management XIV, vol. 212, 1991, pp. 57–64.
[20] T. Chave, Etude des mécanismes d'altération par l'eau du verre R7T7 en milieu confiné, compréhension et modélisation de la cinétique résiduelle. PhD Thesis, Université Montpellier II, Sciences et Techniques du Languedoc, 2008, pp. 1–254.
[21] E. Vernaz, J.L. Dussossoy, Applied Geochemistry 7 (1992) 13–22.
[22] T. Chave, P. Frugier, A. Ayral, S. Gin, Journal of Nuclear Materials 362 (2007) 466–473.
[23] J. Anthony, R. Bideaux, K. Bladh, M. Nichols, Handbook of Mineralogy, Mineralogical Society of America, Mineral Data Publishing, Berlin, 2001.
[24] S. Gin, J.P. Mestre, Journal of Nuclear Materials 295 (2001) 83–96.
[25] S. Ribet, S. Gin, Journal of Nuclear Materials 324 (2004) 152–164.
[26] T. Advocat, J.L. Chouchan, J.L. Crovisier, C. Guy,V. Daux, C. Jégou, S. Gin, E. Vernaz, Borosilicate nuclear waste glass alteration kinetics: Chemical inhibition and affinity control, in: MRS Symposium – Scientific Basis for Nuclear Waste Management XXI, vol. 506, 1998, pp. 63–70.
[27] P. Appere, Altération de pastille de verre et de poudre de verre nucléaire en régime dynamique. Industrial Project Report (Projet industriel), Ecole des Mines d'Alès, 1996, pp. 1–51.
[28] F. Delage, Etude de la fonction cinétique d'un verre nucléaire. PhD Thesis, Université de Montpellier II, Sciences et Techniques du Languedoc, 1992, pp. 1–178.
[29] P. Frugier, S. Gin, J.E. Lartigue, E. Deloule, SON68 glass dissolution kinetics at high reaction progress: Mechanisms accounting for the residual alteration rate, in: MRS Symposium – Scientific Basis for Nuclear Waste Management XXIX, vol. 932, 2006, pp. 305–312.
[30] P. Jollivet, Y. Minet, M. Nicolas, E. Vernaz, Journal of Nuclear Materials 281 (2000) 231–243.
[31] I. Ribet, N. Godon, S. Gin, Y. Minet, P. Jollivet, P. Frugier, E. Vernaz, J.M. Cavedon, V. Petitjean, The $V_0 - V_r$ operational model for the long-term behavior of vitrified R7T7 waste packages, in: Advances for Future Nuclear Fuel Cycles Nimes, Atalante, France, 2004, pp. 1–8.
[32] C. Pozo, O. Bildstein, J. Raynal, M. Jullien, E. Valcke, Applied Clay Science 35 (2007) 258–267.
[33] V. Lagneau, Influence des processus géochimiques sur le transport en milieu poreux: application au colmatage des barrières de confinement potentielles dans un stockage en formation géologique. PhD Thesis, Ecole des Mines de Paris, 2000, pp. 1–186.
[34] A. Vinsot, S. Mettler, S. Vechner, Physics and Chemistry of the Earth 33 (2008) S75–S86.
[35] E.C. Gaucher, C. Tournassat, F.J. Pearson, P. Blanc, C. Crouzet, C. Lerouge, S. Altmann, Geochimica et Cosmochimica Acta 73 (2009) 6470–6487.